DOI: 10.1118/1.4890602

MCTP system model based on linear programming optimization of apertures obtained from sequencing patient image data maps.

A Ureba[1], FJ Salguero[2], AR Barbeiro[1], E Jimenez-Ortega[1], JA Baeza[1], H Miras[3], R Linares[4], M Perucha[4] and A Leal[1]

[1] Dpto. Fisiología Médica y Biofísica. Facultad de Medicina, Universidad de Sevilla, Spain

[2] Nederlands Kanker Instituut (NKI), Amsterdam, Holland

[3] Servicio de Radiofísica, Hospital Universitario Virgen Macarena, Sevilla, Spain

[4] Servicio de Radiofísica, Hospital Infanta Luisa, Sevilla, Spain

Corresponding author:

Prof. Antonio Leal Plaza, PhD

e-mail: alplaza@us.es

Phone: +34.95.455.9864

Fax: +34.954551769

Dept. Fisiología Médica y Biofísica

Universidad de Sevilla

Avda. Sánchez Pizjuán, sn

41009 – Sevilla

Spain

Abstract

Purpose: We present a hybrid direct MLC aperture optimization model exclusively based on sequencing of patient imaging data to be implemented on a Monte Carlo treatment planning system (MC-TPS) to allow the explicit radiation transport simulation of advanced radiotherapy treatments with optimal results in efficient times for clinical practice.

Methods: The planning system (called CARMEN) is a full MC-TPS, controlled through a MatLab interface, which is based on the sequencing of a novel map, called 'biophysical' map, which is generated from enhanced image data of patients to achieve a set of segments actually deliverable. In order to reduce the required computation time, the conventional fluence map has been replaced by the biophysical map which is sequenced to provide direct apertures that will later be weighted by means of an optimization algorithm based on linear programming. A ray-casting algorithm throughout the patient CT assembles information about the found structures, the mass thickness crossed, as well as PET values. Data are recorded to generate a biophysical map for each gantry angle. These maps are the input files for a home-made sequencer developed to take into account the interactions of photons and electrons with the multileaf collimator (MLC).

For each linac (Axesse of Elekta and Primus of Siemens) and energy beam studied (6, 9, 12, 15 MeV and 6MV), phase space files were simulated with the EGSnrc/BEAMnrc code. The dose calculation in patient was carried out with the BEAMDOSE code. This code is a modified version of EGSnrc/DOSXYZnrc able to calculate the beamlet dose in order to combine them with different weights during the optimization process.

Results: Three complex radiotherapy treatments were selected to check the reliability of CARMEN in situations where the MC calculation can offer an added value: A head-and-neck case (Case I) with three targets delineated on PET/CT images and a demanding dose-escalation; a partial breast irradiation case (Case II) solved with photon and electron modulated beams (IMRT+MERT); and a prostatic bed case (Case III) with a pronounced concave-shaped PTV by using VMAT. In all cases, the required target prescription doses and constraints on organs at risk were fulfilled using in a short enough time to allow routine clinical implementation of such a MC-TPS for

similar specialized cases. The quality assurance protocol followed to check CARMEN system showed a high agreement with the experimental measurements.

Conclusions: A Monte Carlo treatment planning model exclusively based on maps performed from patient imaging data has been presented. The sequencing of these maps allows obtaining deliverable apertures which are weighted for modulation under a linear programming formulation. The model is able to solve complex radiotherapy treatments with high accuracy in an efficient computation time.

Keywords: Monte Carlo, Treatment Planning, Direct Aperture, Linear Programming

I. INTRODUCTION

Clinical studies show that a prescription dose deviation of 5% may compromise tumor response and morbidity [1, 2]. The accuracy of dose delivered to the patient is a critical issue that depends on multiple and interconnected stages in the radiation therapy process, but it is considered that the criterion of acceptability for dose calculation algorithms ranged between 2% to 5% in dose [3]. In fact, the dose calculation accuracy in complex and heterogeneous geometries has been increased with different degree of success by means of analytical algorithms such as convolution methods [4], collapsed cone [5], pencil beam [6] with corrections, superposition/convolution[7] or anisotropic analytical algorithm [8]. On the other side, several research groups have developed Monte Carlo (MC) dose engines which have been used as a gold standard for comparative studies [9]. Examples of the latter are, DPM/PENFAST[10], MCDOSE/MCSIM[11], VMC[12], XVMC[13], VMC++[14], PEREGRINE[15], MMC[16] and DOSXYZ[17], among others. Furthermore, some of the mentioned MC codes have been partially included in commercial treatment planning systems (TPS). MC treatment planning (MCTP) can provide a lower uncertainty in dose calculation well within the 3% required for accurate radiotherapy [18].

For photon beams, the analytical algorithms can accurately calculate the dose in most of cases. Nevertheless, MC has been used to validate these algorithms for complex techniques, such as Intensity Modulated Radiotherapy (IMRT) where there is a significant amount of non-standard conditions and where the beam modifiers play an important role in the characterization of the beams composing the modulated fields[9].

Transport through the patient-dependent components such as the field-defining collimators and the multileaf collimators (MLC) should be considered in the optimization process for planning. Unfortunately, the most detailed approach such as full MC based on an explicit radiation transport can be inefficient due to the time required to get a low statistical uncertainty, so different approximation algorithms are usually considered in order to get an efficient simulation [19]. However, for some radiotherapy plans or techniques, the level of approximation of the transport may end up making unjustified the use of MC. Full MC (fMC) simulations, in addition to calculation the dose based on the physical heterogeneities in the patient, make it possible to consider MLC transmission, scattering and secondary particles contributions in order to take into account the physical characteristics of the beam reaching the heterogeneous patient structures [18]. The contribution of scattered and transmission radiation can represent a fraction of the dose in the organs at risk (OAR) of the patient and should be considered by TPS algorithms [19, 20]. Without doubt, fMC simulation is a powerful tool to properly characterize the linac beam quality and for patient dose calculation, taking into account the most important physical processes involved in the problem of the planning process. However, fMC implies computationally time consuming simulations of the geometry of each segment or aperture of an IMRT, and it is still not considered as a routine clinical solution despite of the parallel computing solutions available today.

Apart from these points, techniques with many incidence beams, such as Volumetric Modulated Arc Therapy (VMAT) and dynamic IMRT approaches based on sliding windows, do not necessarily require a time longer for MC simulation than the time spent for simple treatments with fewer beams, while analytical algorithms take a longer time when increasing number of incidence beams. In this cases, a limited number of histories are required for each individual beam contribution, as it is the final dose due to the sum of all beams that should provide enough statistics[18].

The delivery and the corresponding verification of VMAT treatment planning are conceptually similar to those of IMRT[21]. These techniques, because of the higher complexity involved, are more prone to be inadequately planned and delivered, so MC could be an excellent tool for treatment quality assurance (QA)[22].

Besides the use of variance reduction techniques and parallel computing, the problem of time consuming associated to MCTP can be overcome by the successful combination of algorithms along the optimization process that are appropriate to the

characteristics of the MC simulation. Surely, MC never will be efficient enough, if we face the optimization problem in the same way as traditionally it has been done with the analytic algorithms. From now on, we will try to expose the essential characteristics that we believe the optimization algorithm has to implement to achieve a treatment planning system based on explicit MC simulation that could be used efficiently in the clinical routine.

Once the statistical uncertainty is established, the necessary number of histories to reach a precise dose distribution is related to the total number of voxels (dose points) and to the total number of incident beams (beamlets) with specific monitor units. A reduction of the number of beamlets and/or voxels simplifies the initial problem and makes it possible to decrease of the overall treatment planning time.

In order to reinforce the idea of reducing the initial conditions of the optimization problem, it could be interesting to introduce a direct aperture optimization model (DAO)[23]. The approach of DAO has been applied to both IMRT as well as VMAT [23], with the main purpose of incorporating MLC properties directly into the optimization process. In this manner, it is expected to obtain apertures inherently deliverable and to involve fewer segments and monitor units (MU) than with the traditional sequenced fluence map [23]. Basically, the algorithm optimizes the MLC aperture shapes and weights using a probabilistic metaheuristic method, generally simulated annealing, to minimize dose-volume objective functions. DAO was developed for inverse planning and requires a previous calculation of dose in the patient in such a way that the algorithm must decide at each iteration whether the new proposed MLC positions and weights improve the previous dose distribution. MC has already been associated to DAO approach [24]. Although some dosimetric properties due to the MLC can be included in the optimization process, is not possible to consider previously the explicit simulation of a geometry which has not been found yet. For a time-efficient optimization, while still considering sources of uncertainties such as leakage, head scatter and tongue-and-groove effect it could be desirable to bypass the traditional inverse optimization, and instead of it, directly optimize only the weights of direct apertures. Class solutions[25] or few direct segments created by an anatomy-based segmentation tool[26] may be an option to replace the classical sequencing process. The reduction of control points seems to be a convenient approach for an explicit MC simulation of the linac geometries. Also, this reduction relies not only on the low number of geometries to be simulated, but also on making dispensable the

previous dose calculation of corresponding beamlets to generate the initial intensity map. Anatomy-based approaches are implemented in commercial algorithms showing a high speed of treatment planning and an efficient use of MUs, but it is usually at the expense of a degradation in the plan quality [27]. Anatomy-based concept is carried out by means of the beam´s eye view of the structures for a combination of them. No leaf-sequence algorithm is applied to modify the aperture shapes, so the initial selection of these apertures determines the rest of the planning.

In this work, we present an optimization treatment model based on the same idea than patient anatomy based algorithm and including more information from the patient image data in addition to the projection of structures. In this way, we generate maps as demanding as the conventional fluence maps, so a sequencing process is necessary and advisable. Basically, our model establishes imaging data as the unique information required for finding apertures before the weighting process, so the implementation of these image maps does not mean to discard a sequencing process, which is a fast process. The main goal is to avoid the previous dose calculation of beamlets or draft apertures and so, allow an explicit simulation of the beam modifiers in an efficient manner.

On the other hand, it is also possible to reduce the size of the initial optimization problem by selecting only a set of dose points to optimize, instead of all of them, such as they are considered when dose-volume constraints are implemented in the inverse planning. This selection can be done randomly or considering those voxels directly involved in the complexity of the relative dose distribution, for example, the voxels in the intersection of PTV and a specific OAR.

Recently, some research groups have made efforts to recover the idea of formulating the optimization problem of beam weighting as a system of linear equations [28-31]. Linear functions and piecewise linear convex objectives and constraints can be solved with linear programming (LP). Dose-voxel optimization model can be written under LP formulation, in which each voxel can be identified in the objective function. In spite of the fact that the number of voxels can be reduced with LP formulation, it has been not commercially implemented because the usual inverse planning implies many beamlets and therefore, the number of equations involved is unfeasible [32]. Nevertheless, the replacement of conventional beamlets by few apertures can significantly reduce the number of equations involved in a LP formulation and so,

making possible to take advantage of considering and imposing dose constraints at the voxel scale. Moreover, this formulation is naturally more suitable for a dose painting by number approach to be applied according to functional and molecular information assessed by combined PET/CT imaging.

In order to show the feasibility of explicit simulations for clinical routine, a full MC treatment planning (MCTP) system model, called CARMEN, has been developed by our group. For each incidence angle, direct apertures are generated from the sequencing of a novel biophysical map composed by imaging data of the patient, instead of a traditional fluence map. This biophysical map is generated by means of an algorithm, called Biomap, able to combine matrixes corresponding to different aspects of the image, which relative importance in the map can be controlled by means of specific parameters, in order to keep the trade-off between the homogeneity and coverage of PTV, and degree of modulation for a better OARs sparing. The weighting optimization of the apertures is carried out by a voxel-based LP optimization model. This MCTP model is able to be specifically applied for planning complex radiotherapy treatments using modulated electron and photon beams. For this work, several actual clinical cases involving different complications were planned by using CARMEN system. The cases were solved with optimal dose distribution while keeping the computation time at acceptable levels in addition a high agreement with the experimental verification.

II. MATERIAL AND METHODS

II.A. CARMEN system algorithm

CARMEN system can work under different planning mode: one following a conventional model based on inverse planning and other model based on DAO, specially designed for a time-efficient explicit simulation. The first mode uses MC simulations of phase-space data (PSD) previously divided into small rectangular regions in order to generate a grid of finite-sized beamlets for an inverse optimization process able to find the corresponding weights to produce a fluence or intensity map for each beam. This working mode already proved good results for complex situations, in which was not possible to use the conventional planning systems, such as the case of using mixed electron and photon modulated beams for breast cancer [33, 34].

In this work we present the second mode, which is based on direct apertures initially generated for each field incidence by means of the sequencing of a matrix composed by mass thickness values, clinical structures of interest and/or image intensities of PET. This matrix, henceforth 'biophysical map', is a combination of all information according to certain criteria managed by means of the Biomap (BM) algorithm, which will be described later.

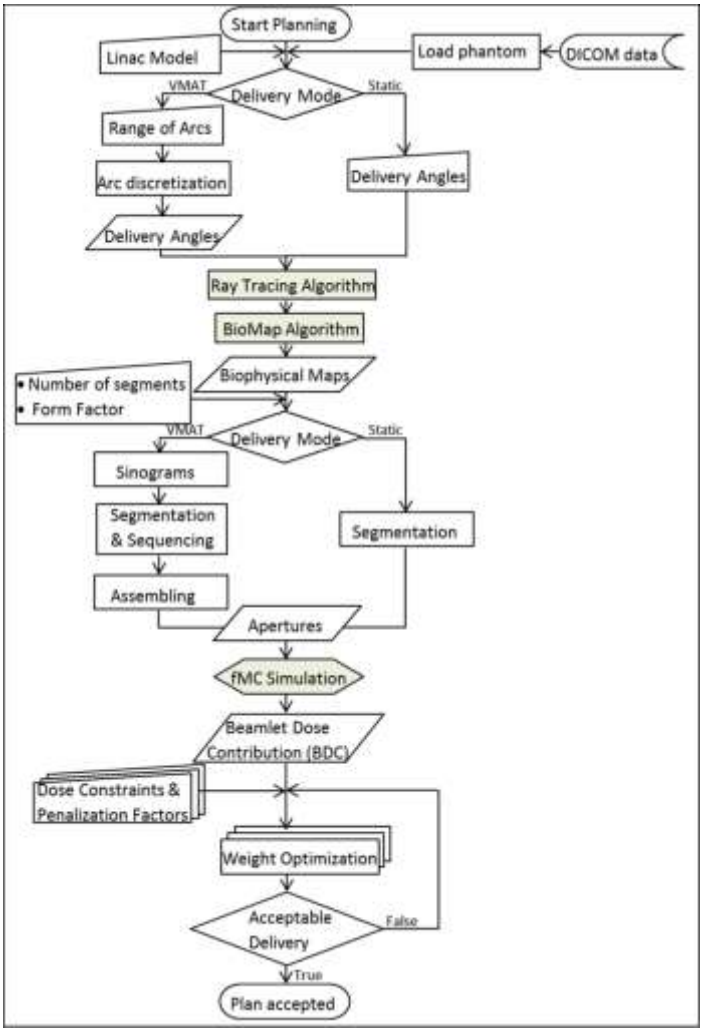

FIG. 1. CARMEN planning system workflow.

The biophysical maps are obtained following a beam's-eye-view (BEV) based search of the CT or PET/CT images for specific incidences or arcs, depending on the chosen radiotherapy technique. The sequencer is based on simulated annealing (SA) and the beamlet weighting factor adjustment is calculated by means of LP formulation. In this way, the planning takes into account interaction effects with linac modifiers by MC simulation. A workflow schema is presented in Fig. 1.

CARMEN planning workflow consists of three different stages: generation of biophysical maps and sequencing to find the direct apertures; MC simulation of the apertures and the corresponding dose calculation to be used as beamlets; voxel-based optimization process based on LP formulation.

II.A.1 Generation of apertures from a biophysical map

In the first step of the optimization procedure, an initial set of matrices is generated by means of a simple voxel traversal algorithm for ray tracing. For each incidence, this algorithm generates 2-D matrices with the projections from the BEV of structures of interest. Each one of these matrices has a grid resolution limited in one direction by the leaf size at the isocenter and by a user-dependent parameter in the other direction. Collimator angle and isocenter point are selected from this first stage. The collimator angle for VMAT cases is constant along each arc, but it can be changed for static IMRT cases. When the collimator angle is changed, the projection of structure is what really is adapting to the calculation grid in order to keep the same resolution. Based on these matrices, an algorithm called Biomap, has been developed to prepare the biophysical maps, which will be sequenced in order to obtain the apertures needed for the weighting optimization process.

In Fig. 2, we present an example to show the performance of Biomap algorithm. The biophysical map (Fig. 2(b)) corresponding to the incidence 23 (220º) of an IMRT case is the input for our sequencer in order to find the apertures (Fig. 2(c)) able to achieve the desired dose distribution after weighting optimization process. The information concerning the OARs crossed by the ray path contributes to the accumulated values on the biophysical map depending on the type of structure, its relative position in the path (in front or behind the PTV) and even on the associated level of toxicity to each structure. The mass thickness value is obtained by considering the exponential function attenuation corresponding to each physical density in the voxels when they are crossed by photon beams. For electron beams, the distance from the body to the bottom of the target is considered in order to select the energy beam according the electron therapeutic range. Biomap algorithm works with matrices and parameters which specific values for the example can be seen in Fig. 2. An extended explanation of the algorithm is given below.

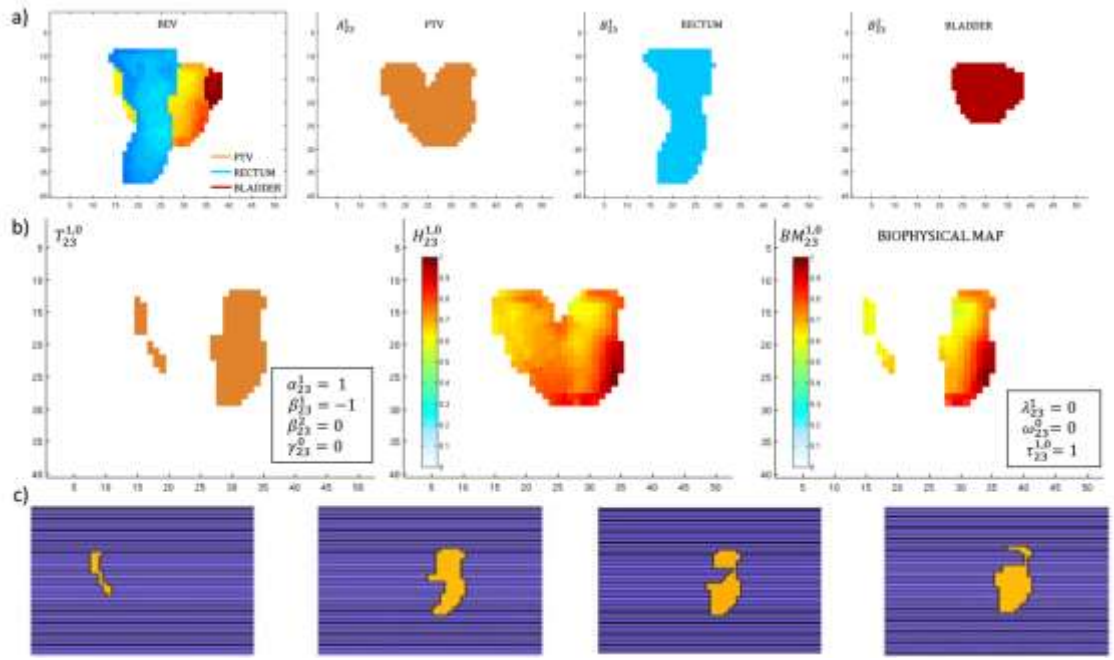

FIG. 2. For incidence 23 (220°), as an example, ray casting algorithm provides one Target (*l*=1), two OARs (m=1, 2), and no PET values (*r*=0). In a) the different structures with the corresponding matrices to be combined are shown. In b) are presented the matrices needed to generate the corresponding biophysical map and the latter in the right side. In c) are represented the apertures obtained with the sequencer. Form factor was strongly considered, the number of levels was set to 3 and the number of segments per level was set to 2.

Biomap algorithm:

Once beam angles of each incidence and the structures of interest are specified, our ray casting algorithm provides one map for each structure for each incidence with *MxN* dimension, being *M* the leaves collimator number and *N* the resolution of leaf movement.

$$\text{Let } A_k^l, B_k^m, C_k^r, E_k^{l,r} \in M_{MxN} \quad \forall k = 1,2,\dots,\text{Number of incidences}$$
$$\forall l = 0,1,2,\dots,\text{Number of targets}$$
$$\forall m = 1,2,\dots,\text{Number of OARs}$$
$$\forall r = 0,1,2,\dots,\text{Number of PET values}$$

Let incidence k (different incidence values could present the same angle value) A_k^l, B_k^m and C_k^r are the projected maps for the target l, the m OARs and the PET value r, respectively. Note that a specific PET value usually represents a SUV value and r is the index representing the number of different SUV values considered for each case. $E_k^{l,r}$ represents the mass thickness map for either the target l or the specific PET value r. If no PET values are available its relative parameters and matrices are null. An example to explain some of the parameters involved in BIOMAP is shown in Figure 2(a). A, B and C are projection maps, indeed their elements are 0 or 1. However, E

elements are positive real numbers and represent the mass thickness seen from each grid element.

To consider the different attenuation through the tissue we define $H_k^{l,r}$.

For each l, r and k, let $\left(H_k^{l,r}\right)_{ij} \equiv 1 - e^{-\mu\left(E_k^{l,r}\right)_{ij}}$, $H_k^{l,r} \in M_{MxN}$ (1)

μ is the mass attenuation coefficient of the tissue, indexes i and j are the elements of the matrix H, corresponding to the positions of the projection grid. As an approximation, μ is a constant for all tissues. Note, when using electron beams we consider H=E.

The matrix working as a mask, $T_k^{l,r}$, is calculated from a set of parameters called α_k^l, β_k^m, γ_k^r related to the target l, the m OARs and the PET value r, respectively (Figure 2(b)). This matrix by means of the combined matrix $X_k^{l,r}$ is generated to take into account potential overlapping of structures and the relevance of them for planning of the specific incidence k. $X_k^{l,r}$ is the combination of A_k^l, B_k^m and C_k^r.

For each l, r and k, let

$$X_k^{l,r} \equiv \left(A_k^l, B_k^1, \dots, B_k^m, C_k^r\right) \cdot \begin{pmatrix} \alpha_k^l I \\ \beta_k^1 I \\ \vdots \\ \beta_k^m I \\ \gamma_k^r I \end{pmatrix}, \; I \in M_{NxN}, X_k^{l,r} \in M_{MxN} \quad (2)$$

$$\alpha_k^l + \gamma_k^r = 1 \qquad \alpha_k^l, \gamma_k^r \in \{0,1\} \qquad (3)$$

$$\beta_k^m \in [-1,0]$$

$$\left(T_k^{l,r}\right)_{ij} \equiv \begin{cases} \left(X_k^{l,r}\right)_{ij}, & \left(X_k^{l,r}\right)_{ij} \geq 0 \\ 0, & \left(X_k^{l,r}\right)_{ij} < 0 \end{cases}, \; T_k^{l,r} \in M_{MxN} \quad (4)$$

$$D_k^{l,r} \equiv T_k^{l,r} \cdot H_k^{l,r}, \; D_k^{l,r} \in M_{MxN} \quad (5)$$

I is the identity matrix. $D_k^{l,r}$ is the matrix with the information obtained from the BEV following a relevance criteria and considering the mass thickness (Fig. 2 (b)). Note that β_k^m parameters allow us to consider different OARs toxicity levels for each incidence k.

The biophysical map (BM) previous the sequencing process for the incidence k, is a selection between matrices for coverage purpose (A_k^l and C_k^l) and modulation purpose ($D_k^{l,r}$). Therefore, $BM_k^{l,r}$ is defined as follows:

$$BM_k^{l,r} \equiv \left(A_k^l, C_k^r, D_k^{l,r}\right) \cdot \begin{pmatrix} \lambda_k^l I \\ \omega_k^r I \\ \tau_k^{l,r} I \end{pmatrix},\ BM_k^{l,r} \in M_{MxN} \quad (6)$$

$$\lambda_k^l + \omega_k^r + \tau_k^{l,r} = 1 \qquad \lambda_k^l, \omega_k^r, \tau_k^{l,r} \in \{0,1\} \quad (7)$$

λ_k^l, ω_k^r and $\tau_k^{l,r}$ are a set of parameters to let the selection commented above. In this way, each BM can be designed to obtain apertures for target covering or for sparing the OARs (Fig. 2(b)).

This algorithm was designed to allow the control of a set of parameters (α_k^l, β_k^m, γ_k^r) and (λ_k^l, ω_k^r, $\tau_k^{l,r}$), related with the disease site and the specific schema of toxicity levels. These parameters allow take into account the relative importance between different goals, such as coverage, or modulation. In this way, the finding of class solutions or templates to be applied to recurrent cases is expected.

A home-made sequencer [33] takes into account user parameters such as the Form factor (ratio area-perimeter), number of segments for each intensity level and the number of intensity levels for each biophysical map. The sequencer consisted of a multi-objective minimization through a simulated annealing algorithm and it was already successfully for other works [33, 34]. It was designed to find apertures also for electron beams, by considering the different interaction of the particles with the leaves. Each intensity level represented a range of values in the biophysical map according to different aspects in the image data. This intensity can correspond to mass thickness or distance from body to PTV, the weighted projection of an OAR or the SUV value from a PET study. Each matrix defined in the Biomap algorithm, is related with these different aspects of the image in such a way that is necessary to establish the relative importance between them. Once the priorities are established by the user by selecting a set of parameters, the Biomap algorithm generates the biophysical map ready for the sequencing.

The sequencer provides the set of apertures or segments that will be explicitly simulated (Fig. 2(c)). VMAT cases require interconnectedness of the beam shapes as the gantry rotates so, in this case, the sequencer works on the sinogram for each leaf, which are generated from the set of Biomaps along the arc. Other approaches like

sweeping windows and complementary apertures algorithm [35] are also implemented for VMAT.

II.A.2. Monte Carlo simulation of apertures and dose calculation

The EGSnrc Monte Carlo user code BEAMnrc[36, 37] was used to simulate a 6MV photon beam from a Siemens Primus linac and its electron beams of 6, 9, 12, 15 and 21 MeV, as well as, a 6 MV photon beam from an Elekta Axesse linac. For photon beams, a PSD file was previously obtained at the exit of the patient-independent components of the linac head (Target, Primary collimator, flattening filter, monitor chamber, backscatter plate, mirror and secondary collimator for Axesse model) to use as source for the transport simulation through the patient-dependent components (JAWS, MLC and fixed diaphragms for Axesse model) which are variable for each treatment.In this way, it is possible to save the time spent for the subsequent repetition of this simulation stage common for each treatment. For electron beams, the mentioned PSD source file was not generated because the computation time saving is negligible when facing the whole simulation transport of the linac head, especially thanks to the lack of components such as target and flattening filter. In this case, only the components for the irradiation of electron beams present in the linac head of Primus model were modeled, including specific components for electrons such as scattering foil.

The apertures shape was defined by jaws and/or MLC, except in the case of electron beams, where the fields are only shaped with the MLC, and the jaws are fully retracted to reduce scattering. This last configuration has already been used successfully by our group for modulated electron radiotherapy (MERT)[33, 34].

The following BEAMnrc transport parameters were employed: NIST for bremsstrahlung cross sections; EXACT as boundary crossing algorithm and PRESTA-II as electron-step algorithm; for Bremsstrahlung angular sampling, the leading term of Koch-Motz distributions was chosen; electron and photon cutoff energies were 0.7 MeV (0.189 MeV kinetic energy) and 0.01 MeV, respectively.

Electron range rejection with an energy cut-off of 2.0 MeV was implemented in the photon beams simulations. Directional Bremsstrahlung Splitting was activated to obtain the first phase-space data file, which was used as the input for the simulation of the part of the patient-dependent linac head geometry. For electron beam simulations,

electron range rejection was not used.

The PSD files corresponding to each aperture were obtained below the MLC. These PSDs were used as source for dose calculation by means of a modified version of DOSXYZnrc[38], named BEAMDOSE[33]. This modification allows knowing every aperture contribution to each voxel in order to score the beamlet dose contribution (BDC) for weighting optimization purpose. For each modeled linac a conversion factor from MC dose to Monitor Units has been calculated by means of experimental measurements[39].A grid calculation consisting on 256 x 256 voxels per slice was used, which meant a high resolution dose calculation but also incremented the computation time. Specifically, the dose calculation of case I was simulated in voxels with 0.18 x 0.18 x 0.5 cm^3, case II with 0.18x0.18x0.5 cm^3, and case III with 0.22 x 0.22 x 0.2 cm^3. For the dose calculation in the patient, the electron and photon cutoff energies were 0.521 MeV and 0.01 MeV, respectively.

Although other grid resolutions are available, we decided to use a high resolution grid to be able to perform a more detailed comparison and to check the model studying CPU times under the most demanding situations.

The number of histories in the PSD corresponding to each aperture was chosen to satisfy a spatial density of 10^5 particles/cm^2 for cases I and II, and of $2 \cdot 10^4$ particles/cm^2 for case III, trying to avoid latent error in order to obtain an adequate statistical uncertainty in final dose per voxel for the optimization and evaluation processes. For each case, the sum of all beams ensured a statistical uncertainty in final dose per voxel (in and around the PTV) lower than 2%.

II.A.3. Optimization algorithm

The optimized weights are calculated by a linear programming algorithm that uses dose prescriptions and constraints together with the matrix BDC. Optimization based on LP for planning [31], provides a linear multi-objective penalty function that avoids local minimum and, unlike other conventional algorithms, provides the possibility to distinguish each voxel individually within the volumes involved in the planning. LP is able to consider more than one target, so it is well suited for simultaneous integrated boost treatments and for planning with several prescription doses based on biological data from PET studies. Moreover, the use of LP facilitates the use of an optimization

based on dose painting by numbers. In addition, the ability to consider each individual voxel allows us to simplify the initial problem by means of a selection of voxels in a specific region or considering only a representative randomized sample of them to represent a whole volume. Thus, the computation time is significantly reduced by considering a reduced number of voxels.

The mathematical formulation of our linear programming model is:

$$o.f. \sum_{i=1}^{N_{org}} P_i \sum_{j=1}^{N_{vox}^i} x_j^i + \sum_{i=1}^{N_{org}} Q_i \sum_{j=1}^{N_{vox}^i} y_j^i \quad (8)$$

$$subject\ to \begin{cases} \sum_{j=1}^{N_{total\ beamlets}} \omega_j B_{kj} - x_k^i \leq D_k^i & k = 1, \dots, N_{vox} \\ \sum_{j=1}^{N_{total\ beamlets}} \omega_j B_{kj} + y_k^i \leq d_k^i & i = 1, \dots, N_{org} \end{cases} \quad (9)$$

where P_i and Q_i represent upper and lower dose penalization factors for each i region; x^i and y^i are overdose and underdose vectors, respectively; B_{kj} and ω_j are the coefficients of the BDC matrix and weight vector corresponding to the beamlets, respectively. D_k^i and d_k^i represent the required maximum and minimum dose user-specified thresholds for each region, respectively. N^i_{vox}, N_{vox} and N_{org} indicate the number of voxels of i region, total number of voxels and total number of regions of interest, respectively.

In order to solve this equation system, we use the free software package GNU Linear Programming Kit (GLPK) when Simplex algorithm is used, or the PCx package[40] when the Interior-Point algorithm is used for those cases where the problem size allows it. Under distributed computing environment, the planning model presented allows executing several simultaneous optimization processes with different sets of parameters by changing dose constraints and/or penalty factors, in order to obtain the best solution based on the DVHs and dose distribution curves comparison.

II.B. CARMEN platform

Our model is supported over an interface based on MatLab. MatLab was selected as the software tool for this project because it is an interactive system that provides wide use of specialized toolboxes such as image processing toolbox, DICOM data acquisition, parallel computing, wavelet packages, etc; besides the ease for manipulating multidimensional data and a simple Sintax [41]. Other of the main reasons to use MatLab was the possibility to compile applications into a stand-alone graphical user interface (GUI) program. CARMEN platform is able to write the MC

455 solutions in a format compatible with the commercial treatment plan standards in order to be imported/exported in the network oncology information system. CARMEN also allows a convenient interface for personnel use by means of a MatLab graphical user interface (GUI) developed with MatLab GUIDE. This platform was designed by our group for planning and experimental verification, in order to streamline, automate and
460 control a fair benchmarking, taking the MC simulation as a reference versus commercial analytical solutions and results derived from experimental measurements. It should be mentioned that the Evaluation mode in CARMEN presents a front-end more refined than the Planning mode, which is under construction to include classical visualization tools for helping the planning process. This GUI provides a user-friendly
465 environment on MatLab to import DICOM format files of CT and PET scans, including delineated structures, dose distributions and planning parameters, and convert them into specific formats for the use of MC code.

This platform can manage the PET/CT co-registration and includes tools to allow users to remove the CT table or fiducial marks, override densities, generate new
470 structures, or merge them with others imported from the DICOM files. For the plans evaluation, a simultaneous display of isodoses corresponding to different plans and/or experimental measurements is provided, in addition to auxiliary interfaces for representing dose volume histograms, gamma analysis and profiles along a dose distribution. CARMEN enables the evaluation of the effects related to changes in the
475 resolution of the calculation grid, as well as those due to the denoising and smoothing strategies applied. Several filtering approaches are implemented in the platform, including specific MC denoising techniques [42]. The code handles the possibility of using parallel programming techniques using the capacity of MatLab multicore and, in a near future, CUDA technology present on graphics processing units (GPU). The
480 computation times presented in this work were achieved with CARMEN installed on a HP Proliant DL585 G7 server with four processors AMD Opteron™ 6174 2.19 GHz with 12 cores (48 independent CPUs), and the simulation tasks were distributed using a coarse-grained parallelization model[43].

485 **II.C. Clinical cases and experimental verification**

In order to verify the feasibility of CARMEN system, we present three different cases chosen to show the possibilities of our proposal in those situations where the MC

simulation can offer an added value, i.e., in non-standard conditions from a dosimetric point of view, and/or under the need of using special techniques only available in the scope of MC treatment planning. The cases were compared to experimental verification corresponding to a quality assurance (QA) protocol in order to validate the Monte Carlo solutions. This QA consisted of the standard gamma analysis based on the distance to agreement (3mm)/dose difference (3%) criteria and a 95% passing rate, by applying a multi-plane verification using the I'mRT Phantom of IBA Dosimetry with Gafchromic EBT3 film. One of the cases was experimentally verified using an ad-hoc breast phantom with semi-spherical geometry. The phantom called NAOMI was especially designed by us for the experimental verification of MERT applied to breast cases and consists of 5mm-thick high-impact polystyrene slabs which can be placed one on top of each other to emulate breasts of different sizes. NAOMI allows placing different types of ionization chambers and radiochromic film at different depths. Absolute dosimetry was measure at the isocenter point or at a representative point in the case with multiple isocenters, with a plane-parallel Roos chamber PTW 34001 for electron beams and ion chamber Wellhoffer CC04 for photon beams. Our acceptance criteria is that the theoretical absolute dose does not must present more than 3% of relative error while considering the experimental measure as reference value.

Case I:

The first case was a head-and-neck cancer patient with three targets due to a non-uniform dose prescription for a biologically heterogeneous tumor. FMISO-PET images were used to determine hypoxic sub-volumes for planning. This case was selected to check CARMEN capability to solve a demanding dose-escalation case with multiple targets delineated on PET/CT images (Table I).

The tumor volume was prescribed with three different doses. By dividing the tumor in three regions, the resulting subvolumes were small, so the Elekta Axesse linac was chosen to obtain a high resolution with 0.4 cm of leaf width projected at the isocenter. The prescriptions were 60, 72 and 82 Gy, respectively, delivered in 30 fractions. The dose prescriptions and dose limitations are shown in (Table I). The planning objectives were: (1) at least 95% of each target structure must receive its prescription dose;(2) the spinal cord must not receive more than 38 Gy (less than the usually 45 Gy limit for the spinal cord);(3) the hot and cold spots must be minimized.

TABLE I. Multiple dose prescription for case I: HR (Hypoxic Region – PTV82), PTV72, PTV60 and dose constraints for the organs at risk.

Prescribed dose and constraints, case I	
HR (PTV82); D_{95}	$\geq$ 136.7% D_p (82 Gy)
PTV72; D_{95}	$\geq$ 120% D_p (72 Gy)
PTV60; D_{95}	$\geq D_p$ (60 Gy)
Spinal cord; V_{38Gy} (63.3% D_p)	0%
Left Parotid gland; V_{38Gy} (63.3% D_p)	$\leq$ 5%
Right Parotid gland; V_{38Gy} (63.3% D_p)	$\leq$ 5%
Mandible; V_{30Gy} (50% D_p)	$\leq$ 1%

D_y is the dose delivered to y% of the structure volume, V_{xGy} is the volume receiving more than x Gy. D_p is the prescribed dose (60 Gy).

The treatment couch was set at 0° in the treatment plan and had nine coplanar, equally spaced 6 MV beams (200°, 240°, 280°, 320°, 0°, 40°, 80°, and 160°) with a 0° collimator rotation (that means that MLC movement was in cross-plane direction when gantry angle is set to 0°).

Case II:

The second case was a partial breast case planned with photon and electron modulated beams (IMRT+MERT) shaped with the photon MLC. MERT has been previously evaluated, demonstrating to be an efficient alternative for partial breast irradiation, by achieving a good sparing of the organs at risk, such as the lung and heart [34]. Combined modulated electron and photon beams employing the same collimation device such as the MLC can only be calculated accurately by means of a treatment planning based on MC, since the electron beam interaction with the leaves plays an important role for modulation purpose. Electron apertures for two 9 MeV beams were designed to be irradiated with SSD=60cm plus two tangential photon beams with SAD=100cm, which needed in order to cover the deeper part of the PTV. This case was planned to be delivered by a SIEMENS Primus linac. Lumpectomy cavity, PTV and PTV_EVAL (PTV used for plan evaluation), as well as normal structures were contoured following NSABP-B39/RTOG-0413 protocol [44]. Dose prescription was 38.5 Gy in 10 fractions and dose limitations for normal tissues were set following the more demanding limits in this protocol (Table II). The planning objectives were: (1) at least 90% of PTV_EVAL must receive 90% of the prescription dose;(2) less than 60%

of ipsilateral breast should receive more than 19.3 Gy; ;(3) less than 35% of ipsilateral breast should receive 38.5 Gy;(4) less than 15% of ipsilateral lung can receive 11.6 Gy;(5) less than 40% of heart should receive 1.9 Gy; (6) the hot and cold spots must be minimized. The treatment couch was set at 0° in the treatment plan and had four coplanar beams; 9 MeV electron beams (25°, 40°) and 6 MV photon beams (139°, 317°) with a 0° collimator rotation.

TABLE II. Dose prescription for case II and dose constraints with a 5% of tolerance according to the NSABP-B39/RTOG-0413 protocol.

Prescribed dose and constraints, case II	
PTV_EVAL;	
D_{90}	≥ 90% D_p (34.7 Gy)
Dmax	≤ 120% D_p (46.2 Gy)
Ipsilateral Breast	
$V_{19.3Gy}$ (50% D_p)	< 60%
$V_{38.5Gy}$ (100% D_p)	< 35%
Contralateral Breast; $V_{1.2Gy}$ (3% D_p)	0%
Ipsilateral Lung; $V_{11.6Gy}$ (30% D_p)	< 15%
Contralateral Lung; $V_{1.9Gy}$ (5% D_p)	< 15%
Heart; $V_{1.9Gy}$ (5% D_p)	< 40%
Thyroid; $V_{1.2Gy}$ (3% D_p)	0%

PTV_EVAL is the planning target volume used for evaluation, D_y is the dose delivered to y% of the structure volume, V_{xGy} is the volume receiving more than x Gy. D_p is the prescribed dose (38.5 Gy). Tolerance ±5%

Case III:

The third case was a prostatic bed with two OARs: bladder and rectum. The prescription was 60 Gy in 33 fractions of 2 Gy per fraction. The dose prescriptions and dose limitations are shown in (Table III). The planning objectives were: (1) at least 95% of each target structure must receive 95% of the prescription dose;(2) the 50% of the bladder must not receive more than 46.2 Gy;(3) the 60% of rectum must not receive more than 39.6 Gy; (4) and the 20% of rectum must not receive more than 59.4 Gy; (5) the hot and cold spots must be minimized. The treatment couch was set at 0° to deliver one arc of 6-MV beam with a constant 90° collimator rotation (that means, that MLC movement was in in-plane direction when gantry angle is set to 0°).This case was solved with VMAT technique to be delivered by the ELEKTA Axesse linac. This

case was selected to check the performance of discretization level of our approach when trying to solve a complex dynamic treatment characterized by continuous gantry rotation and MLC movement while the beam is on. Although there are new Monte Carlo sources capable of simulating the continuous gantry motion for verification purpose[22], for MC planning purpose we had to discretize the simulation in order to be connected to the optimization process, i.e., 180 apertures equally spaced 6 MV beam were simulated. The QA followed in this work allows us to assess the discrepancy introduced between the discrete plan and the continuous delivery.

TABLE III. Dose prescription and dose constraints for case III.

Prescribed dose and constraints, case III	
PTV; D_{95}	$\geq$ 95% D_p (62.7 Gy)
Bladder; $V_{46.2Gy}$ (70% D_p)	< 50%
Rectum; $V_{59.4Gy}$ (90% D_p)	< 20%
Rectum; $V_{39.6Gy}$ (60% D_p)	< 60%
Femoral Heads (RHF, LHF); V_{45Gy} (68.2%D_p)	0%

D_y is the dose delivered to y% of the structure volume, V_{xGy} is the volume receiving more than x Gy. D_p prescribed dose (66 Gy).

III. RESULTS AND DISCUSSION

CARMEN planning achieved the required prescription dose with enough homogeneity for the target volumes in all the cases, and fulfilled coverage and dose limit criteria. In order to improve the visualization quality of MC results, adaptive anisotropic diffusion denoising technique was applied for smoothing the MC calculated dose distributions[45].

The case I was properly solved in spite of its complexity due to heterogeneous target contoured from a PET study with hypoxia region to receive a higher dose. Hypoxic sub-volume and the rest of target sub-volumes received the specific dose prescription and the normal tissue doses were kept within the predefined limits. In Fig. 3, we present the dose-volume histogram (DVH) and several relative dose distributions obtained with CARMEN for this case. This solution showed to be optimal and comparable to those seen in other references regarding head and neck cases contoured from PET/CT images [46].

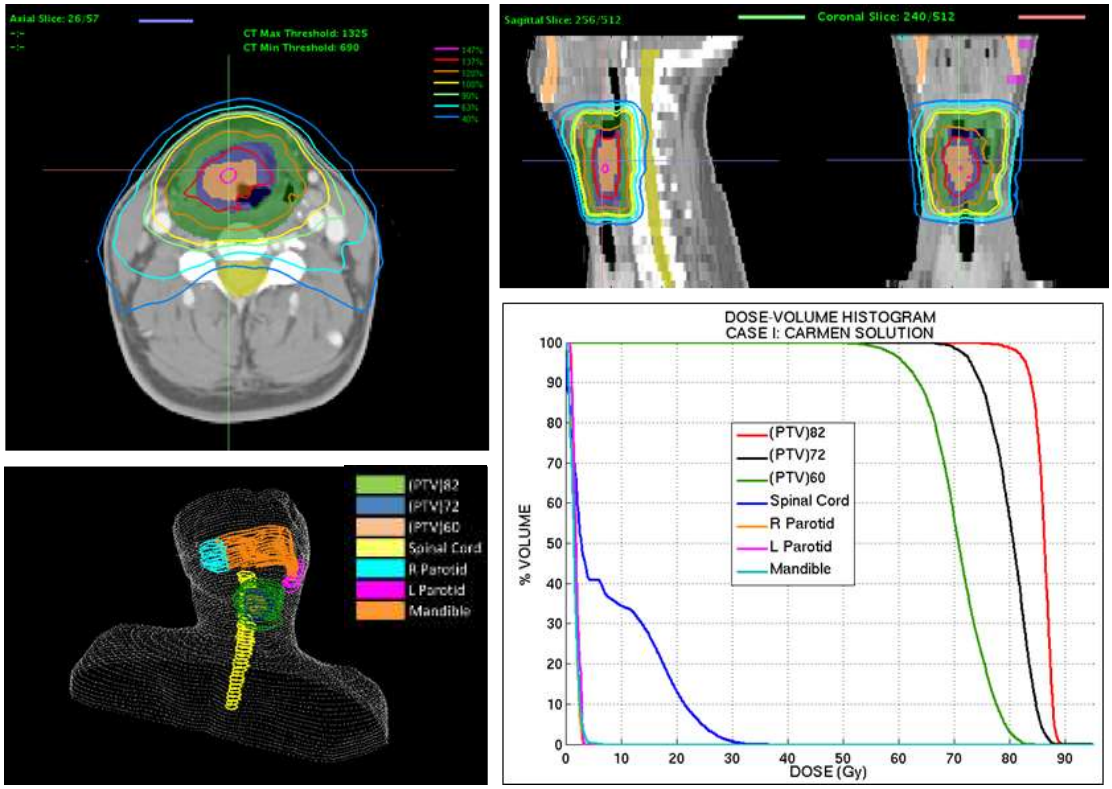

FIG. 3. Dose distributions showing the isolines of 40, 63, 90, 100, 120, 137 and 147% (24, 37.8, 54, 60, 72, 82.2, 88.2 Gy) at the isocenter slice and dose volume histogram obtained with CARMEN for case I.

Case II, a partial breast case, was solved with CARMEN to be delivered by a combination of photon and electron beams shaped by the same computer controlled multi-leaf collimator. Fig. 4 shows the DVH corresponding to the CARMEN solution and isodose lines at a representative plane for this case. The intensity of photon beams, and intensity and energy of electron beams were modulated to achieve higher dose homogeneity within the PTV with a normal tissue, sparing significantly better than the usual for these cases [34].

Case III, corresponding to a complex prostatic bed was planned with VMAT by using only one arc, meaning a short time of irradiation and a lower number of total monitor units. The CARMEN solution achieved lower dose in bladder and rectum, and an adequate coverage of PTV. Fig. 5 shows DVH and isodose lines at the isocenter for the three anatomical planes corresponding to the solution of case III obtained by CARMEN planning.

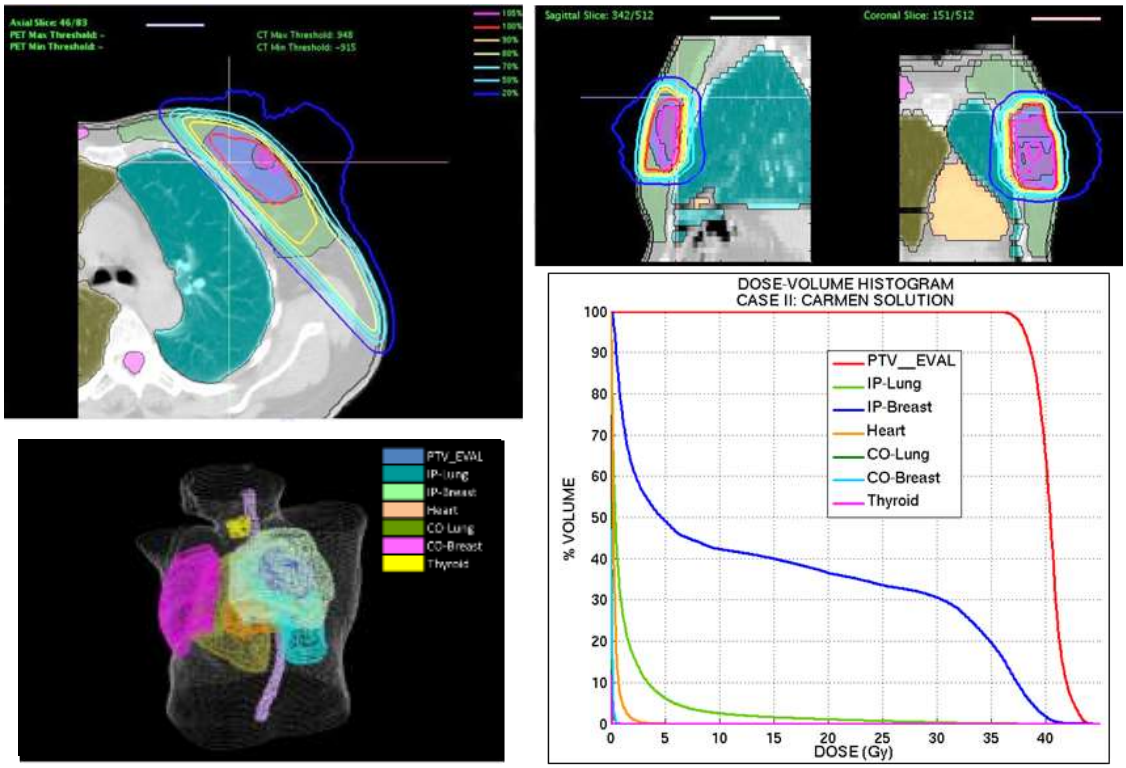

FIG. 4. Dose distributions showing the isolines of 20, 50, 70, 80, 90, 100 and 105% (7.7,19.25, 26.95, 30.8, 38.5, 40.425 Gy)at the isocenter slice and dose volume histogram obtained with CARMEN for case II.

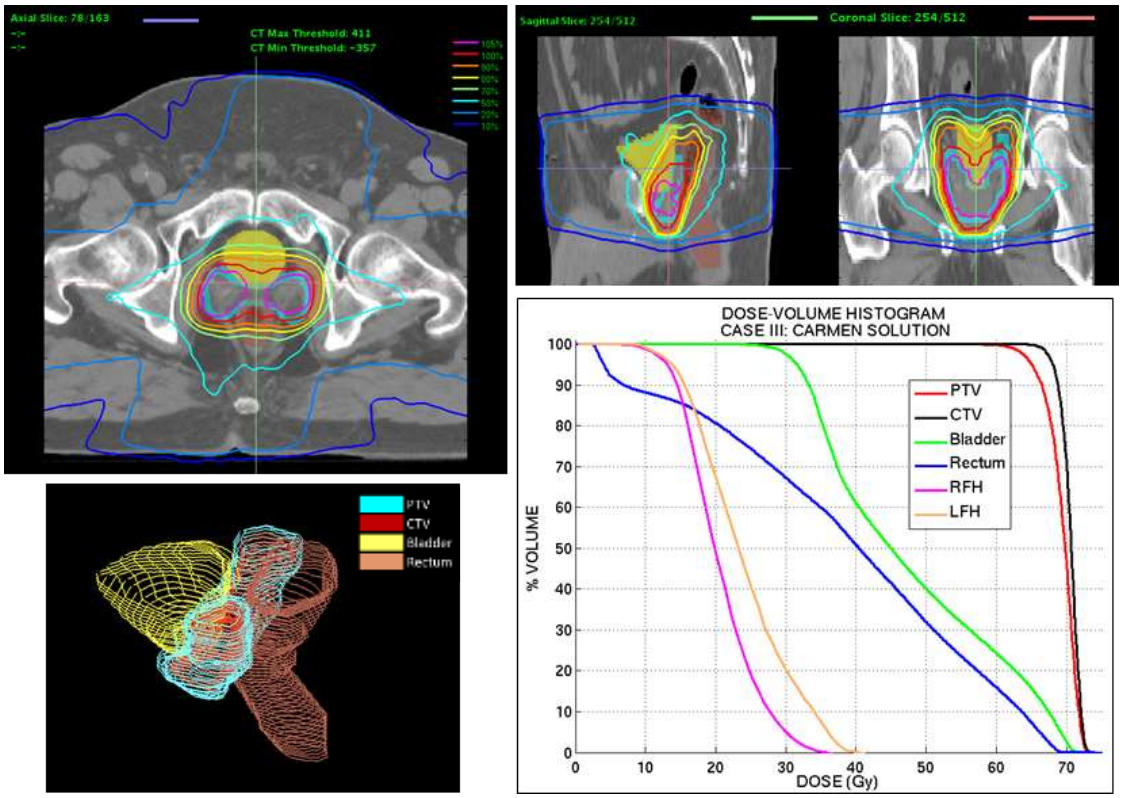

FIG. 5. Dose distributions showing the isolines of 10, 20, 50, 70, 80, 90, 100 and 105% (6.6, 13.2, 33, 46.2, 52.8, 59.4, 66, 69.3 Gy) at the isocenter slice and dose volume histogram obtained with CARMEN for case III.

Table IV shows dose statistics values, such as D_2, D_{98}, D_{mean} and CI (Conformity Index) for targets, and D2 and Dmean for OARs for the three cases presented.

TABLE IV. Dosimetric values planned by CARMEN for case I: HR (Hypoxic Region – PTV82), PTV72, PTV60 and dose constraints for the organs at risk; for case II and dose constraints with a 5% of tolerance according to the NSABP-B39/RTOG-0413 protocol and for case III and dose constraints.

CASE I		CASE II		CASE III	
HR (PTV82)	D_{95} = 83.2 Gy	PTV_EVAL	D_{95} = 38.1 Gy	PTV	D_{95} = 65.0 Gy
8.0 cm^3	D_2 = 88.5 Gy	166.0 cm^3	D_{max} = 44.3 Gy	98.0 cm^3	D_2 = 70.2 Gy
	D_{98} = 86.4 Gy		D_2 = 43.2 Gy		D_{98} = 63.4 Gy
	D_{mean} = 86.0 Gy		D_{98} = 37.3 Gy		D_{mean} = 69.4 Gy
	CI = 0.996		D_{mean} = 40.4 Gy		CI = 0.988
			CI = 0.994		
PTV72	D_{95} = 73.4 Gy	Ipsilat. Breast	$V_{19.3Gy}$ = 37.2%	Bladder	$V_{46.2Gy}$ = 46.4 %
21.3 cm^3	D_2 = 86.4 Gy		$V_{38.5Gy}$ = 5.5%		D_2 = 70.2 Gy
	D_{98} = 71.8 Gy		D_2 = 39.8 Gy		D_{mean} = 47.5 Gy
	D_{mean} = 80.2 Gy		D_{mean} = 14.6 Gy		
	CI = 0.998				
PTV60	D_{95} = 61.0 Gy	Contralateral Breast	$V_{1.2Gy}$ = 0%	Rectum	$V_{59.4Gy}$ = 17.8%
108.8 cm^3	D_2 = 80.6 Gy		D_2 = 0.5 Gy		$V_{38.6Gy}$ = 52.9%
	D_{98} = 57.9 Gy		D_{mean} = 0.1 Gy		D_2 = 67.9 Gy
	D_{mean} = 70.6 Gy				D_{mean} = 39.1 Gy
	CI = 0.984				
Spinal cord	V_{38Gy} = 0%	Ipsilateral Lung	$V_{11.6Gy}$ = 2.2%	Right Femoral Head	V_{45Gy} = 0%
	D_2 = 28.8 Gy		D_2 = 12.6 Gy		D_2 = 31.5 Gy
	D_{mean} = 8.4Gy		D_{mean} = 1.6 Gy		D_{mean} = 20.1 Gy
		Contralateral Lung	$V_{1.9Gy}$ = 0%	Left Femoral Head	V_{45Gy} = 0%
			D_2 = 0.4 Gy		D_2 = 36.5 Gy
			D_{mean} = 0.1 Gy		D_{mean} = 23.4 Gy
Left Parotid gland	V_{38Gy} = 0%	Heart	$V_{1.9Gy}$ = 1.5%		
	D_2 = 3.3 Gy		D_2 = 1.7 Gy		
	D_{mean} = 2.1 Gy		D_{mean} = 0.5 Gy		
Right Parotid gland	V_{38Gy} = 0%	Thyroid	$V_{1.2Gy}$ = 0%		
	D_2 = 3.1 Gy		D_2 = 0.1 Gy		
	D_{mean} = 2.0 Gy		D_{mean} = 0.1 Gy		
Mandible	V_{30Gy} = 0%				
	D_2 = 3.7 Gy				
	D_{mean} = 1.8 Gy				

D_y is the percentage of prescribed dose delivered to y% of the structure volume, V_{xGy} is the volume percentage receiving more than x Gy. D_p is the prescribed dose (60 Gy). CI conformity index (V_{95}/V_{target}).

Table V shows the planning parameters used for all the evaluated cases. It is necessary to remark that the total apertures used for the given solutions were less than those explicitly simulated. Although the sequencing procedure generated 140 and 180 segments for case I and case III, respectively, only 69 and 117 of them had a weight

different than zero after the optimization process. These extra segments consume time for MC simulation, what it could be considered unnecessary. However, the essential goal linked to the first stage of the optimization procedure is to achieve enough degrees of freedom for an efficient weighting, and it is not possible to know *a priori* which apertures will not be finally used, due to being assigned a weight equal to zero.

TABLE V. Planning parameters of CARMEN for the three evaluated cases.

	Planning System	Energy	Gantry Angles	Segments (weight ≠ 0)	MU
Case I	CARMEN (ph)	6 MV	0º, 40º, 80º, 120º, 160º, 200º, 240º, 280º, 320º	140 (69)	579.0
Case II	CARMEN (elec + ph)	9 MeV/ 6 MV	25º, 40º/139º, 317º	5	520.0
Case III	CARMEN (ph)	6 MV	1 arc of 356º (3min. 5 sec.)	180 (117)	375.0

Figures 6, 7 and 8 represent the QA protocol reports corresponding to the experimental verification of the three cases presented in this work. These reports show the dose distributions of only some slices corresponding to the same locations where films were irradiated inside the phantoms, such as it was described in the Material and methods section. Horizontal and vertical profiles and gamma analysis are also included.

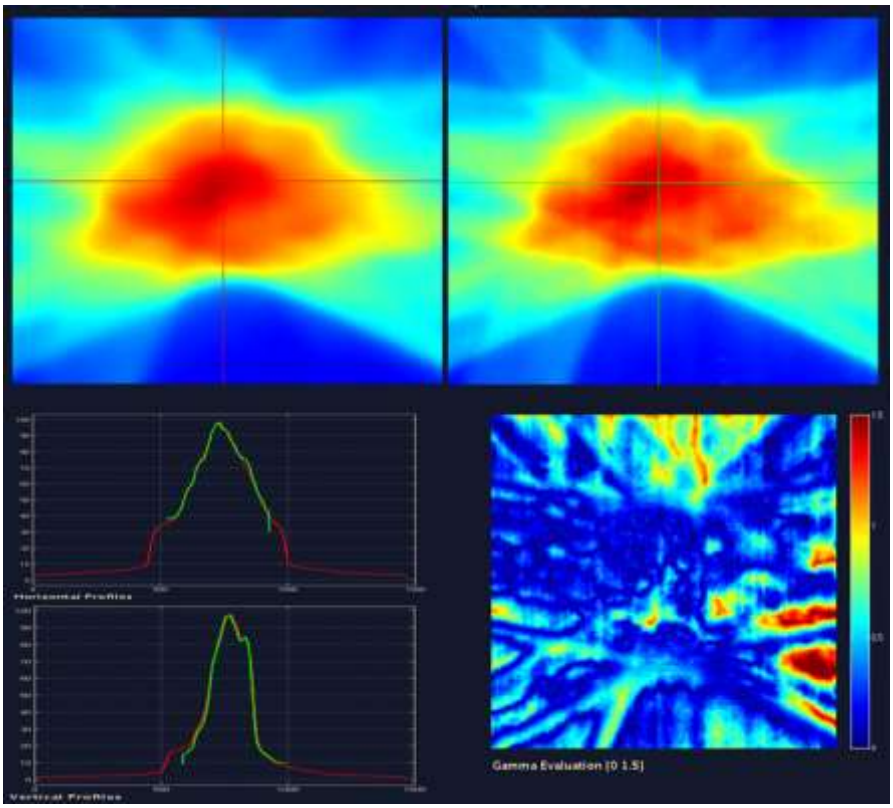

FIG. 6. QA report for case I. Dose distributions corresponding to MC solution (upper left) and to the film (upper right) at the isocenter slice; horizontal and vertical profiles (bottom left) and the corresponding gamma analysis (bottom right).

It is important to note that a scale from 0 to 1.5 was considered only for intuitive gamma visualization, but the gamma index considered was set to 1 for the evaluation criteria (95% of points fulfilling 3mm/3%). No dose threshold was used for gamma analysis, except for the breast case (threshold of 30%) since films in NAOMI phantom were cut flush with the surface of the phantom and the dose in air due to electron beams is not negligible for MC simulation. Anyway, this threshold in case II only excludes those gamma evaluation points quite far from the treatment site, as it can be seen in Fig. 7.

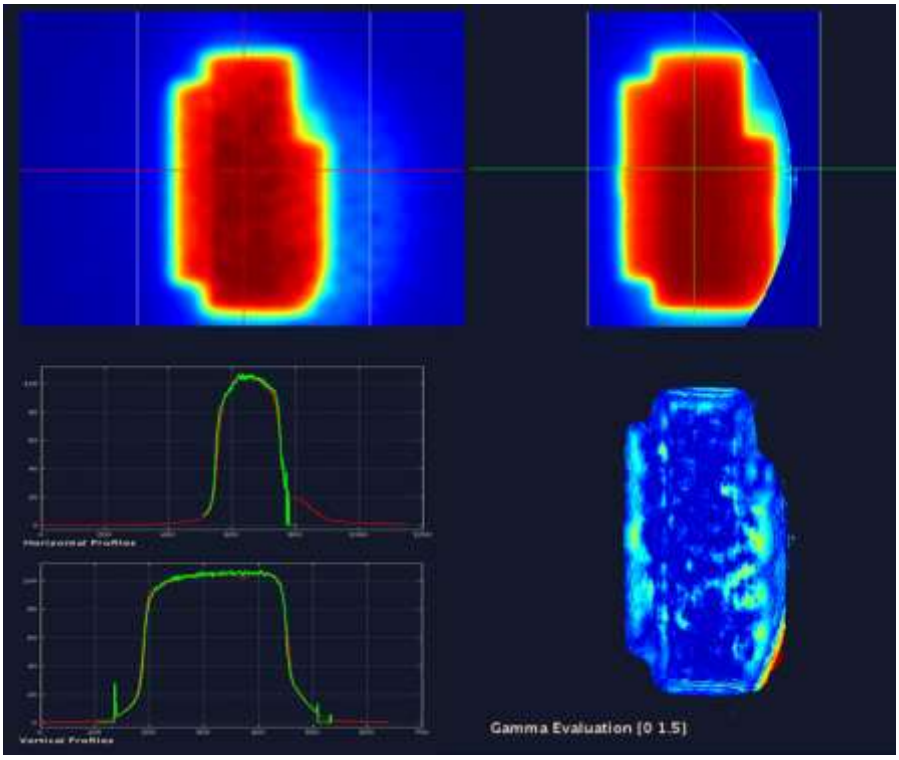

FIG. 7. QA report for case II. Dose distributions corresponding to MC solution (upper left) and to the film (upper right) at a representative slice; horizontal and vertical profiles (bottom left) and the corresponding gamma analysis (bottom right).

A case with volumes as small as the ones considered in case I, forced us to irradiate only 2 films, while in cases II and III, we placed three films in representative slices for these treatments. The percentage of points with gamma values (3 mm distance to agreement and 3% dose difference) lower than 1 was always greater than 95% between CARMEN solutions and the measured values for all films for each treatment.

For absolute dosimetry verification, a point located at the isocenter (at a representative point in case II with two isocenters) was chosen for reference. At this reference point, the doses obtained with the plane-parallel chamber for electron beams and CC04 ion chamber for photon beams agreed with MC calculations within 3%. The resulting

absolute dose verifications, as well as the gamma analysis results for each case are shown in Table VI.

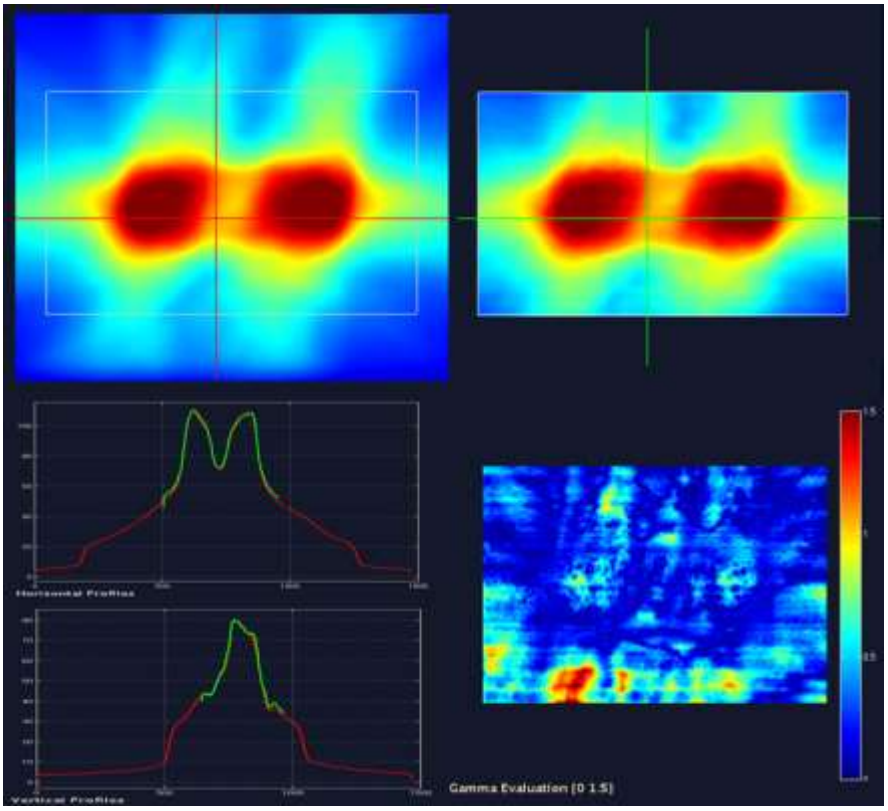

FIG. 8. QA report for case III. Dose distributions corresponding to MC solution (upper left) and to the film (upper right) at 3 cm off isocenter; horizontal and vertical profiles (bottom left) and the corresponding gamma analysis (bottom right).

TABLE VI. Absolute dose verification and global gamma analysis for the three presented cases.

	Experimental dose (cGy)	MC dose (cGy)	Relative error (%) $\frac{D_{MC}-D_{exp}}{D_{exp}}$	Global gamma (%) (3% / 3mm)		
Case I	221.20	226.90	+2.60	96.04	99.53	
Case II	366.61	366.18	- 0.12	97.45	99.18	97.38
Case III	216.10	216.50	+0.16	96.64	96.15	98.56

D_{MC} is the estimated MC dose, D_{exp} is the measured dose.

Finally, the computation times were registered for all evaluated cases. CARMEN system was running on four dodeca-cores processors 2.19 GHz AMD Opteron system (48 independent CPUs). The total planning time spent ranged from one hour to two hours and a half depending of the complexity level of each case. The necessary times spent for each stage in the whole planning process are presented in Table VII.

Excepting for the cases where the number of segments was larger than CPU nodes available, planning time (CPU time) was less than one hour. Regarding the real time necessary for the whole planning process, it is important to remark that beamlets generation is a semi-automatic procedure depending on the case. For VMAT planning it is not necessary any angle selection process, so the apertures selection stage does not increase the process time.

Moreover, as it was commented in Introduction section, to achieve the desired statistical uncertainty in the voxels, the total planning process for VMAT does not require much longer computation time than other cases with less number of apertures, because the total contribution at voxel level can be the same.

TABLE VII. Times spent by the CARMEN system for each planning stage of the cases.

	Apertures generation	Apertures simulation (PSDs)	Dose calculation	Optimization	Total time
Case I	14 min	55 min	18 min	30 min	117 min
Case II	7 min	15 min	30 min	3 min	55 min
Case III	28 min	60 min	56 min	25 min	169 min

IV. CONCLUSIONS

The algorithm proposed in this work implements a novel method for finding apertures based exclusively in the information recorded from the imaging studies previously carried out on the patient. This algorithm is not based on optimization routine for selecting the leaf position by means modification from an initial position. Unlike as DAO works, Biomap sequencing process gives us the definitive apertures for the planning by-passing any inverse process based on a previous dose calculation of beamlets or draft positions of leaves for finding apertures. Therefore, the MC calculation time is only dedicated to explicit simulation transport through the patient-dependent components in the linac head and to obtain the final dose distribution in the voxelized phantom. Moreover, this manner to generate the apertures could be especially efficient for VMAT planification because Biomap algorithm takes the information data from a dynamic BEV in such a way that the apertures are really

deliverable. This study could be carried out in depth for the near future by means of the model presented in this work.

The optimization model presented showed being a suitable and versatile algorithm to be implemented as an alternative in any treatment planning system. Nevertheless, the reduction of initial conditions provided by the model is an excellent way to turn the full Monte Carlo simulation in an efficient tool for radiotherapy planning. Monte Carlo calculation is the best way to theoretically solve the spectral and fluence changes of the beams due to the interaction with modifiers, so it is worthy to reduce computation time and resolve technical problems for its implementation in clinical practice. The efficiency via the reduction of apertures to be simulated by MC also promotes a more transparent and comfortable scenario for the dosimetric verification, which can save time and money invested in the verification of complex treatments, such as VMAT. Nevertheless, MC should always be supported by experimental verification under specific conditions that can ensure a fair comparison regarding the applied grid resolution and well established denoising techniques.

Moreover, the use of fewer apertures allows the reduction of equations for a formulation based on linear programming, which is able to optimize at the voxel level and reduce the dose points in the inverse planning, what is not possible by managing dose-volume constraints. Also, the optimization approach at voxel level makes feasible a future use of our model for the planning based on the dose painting by number. This latter could represent an adequate scenario to develop an accurate adaptive planning based on MC. It is expected that using imaging data as the information to take into account during the optimization process, will allow a planning ready for adaptive radiotherapy in a simple and efficient way, because the adaptive is based on changes of image patient.

ACKNOWLEDGMENTS

This work has been possible thanks to the Spanish Ministry of Science and Technology and the European Community funding (FEDER). We would like to thank Professor Stephen Wright of Computer Sciences Department (University of Wisconsin) for providing us a linear programming solver (PCx). We also wish to acknowledge with gratitude the numerous contributions received from Iuliana Toma-Dasu from Karolinska Institute at Stockholm and Rafael Arráns from the Virgen Macarena Hospital at Seville.

REFERENCES

1. Dische, S., et al., *Precision in reporting the dose given in a course of radiotherapy.* Radiother Oncol, 1993. **29**(3): p. 287-93.
2. ICRU, *Determination of absorbed dose in a patient irradiated by beams of x or gamma rays in radiotherapy procedures.* 1976. **24**.
3. Jacob van Dyk, J.J.B.a.G.S.B., *Accuracy and uncertainty considerations in modern radiation oncology,* in *The Modern Technology of Radiation Oncology*, J.V. Dyk, Editor. 2013.
4. Mackie, T.R., J.W. Scrimger, and J.J. Battista, *A convolution method of calculating dose for 15-MV x rays.* Med Phys, 1985. **12**(2): p. 188-96.
5. Ahnesjo, A., *Collapsed cone convolution of radiant energy for photon dose calculation in heterogeneous media.* Med Phys, 1989. **16**(4): p. 577-92.
6. Ahnesjo, A., M. Saxner, and A. Trepp, *A pencil beam model for photon dose calculation.* Med Phys, 1992. **19**(2): p. 263-73.
7. Ulmer, W., J. Pyyry, and W. Kaissl, *A 3D photon superposition/convolution algorithm and its foundation on results of Monte Carlo calculations.* Phys Med Biol, 2005. **50**(8): p. 1767-90.
8. Tillikainen, L., et al., *A 3D pencil-beam-based superposition algorithm for photon dose calculation in heterogeneous media.* Phys Med Biol, 2008. **53**(14): p. 3821-39.
9. Fogliata, A., et al., *On the dosimetric behaviour of photon dose calculation algorithms in the presence of simple geometric heterogeneities: comparison with Monte Carlo calculations.* Phys Med Biol, 2007. **52**(5): p. 1363-85.
10. Sempau, J., S.J. Wilderman, and A.F. Bielajew, *DPM, a fast, accurate Monte Carlo code optimized for photon and electron radiotherapy treatment planning dose calculations.* Phys Med Biol, 2000. **45**(8): p. 2263-91.
11. Ma, C.M., et al., *Clinical implementation of a Monte Carlo treatment planning system.* Med Phys, 1999. **26**(10): p. 2133-43.
12. Kawrakow, I., M. Fippel, and K. Friedrich, *3D electron dose calculation using a Voxel based Monte Carlo algorithm (VMC).* Med Phys, 1996. **23**(4): p. 445-57.
13. Fippel, M., *Fast Monte Carlo dose calculation for photon beams based on the VMC electron algorithm.* Med Phys, 1999. **26**(8): p. 1466-75.
14. Kawrakow, I., *VMC++, electron and photon Monte Carlo calculations optimized for radiation treatment planning in ''Advanced Monte Carlo for Radiation Physics, particle transport simulation and applications''.* Proceedings of the Monte Carlo 2000 Conference, Lisbon, October 2000, 2000: p. 229-236.
15. Hartman Siantar, C.L., et al., *Description and dosimetric verification of the PEREGRINE Monte Carlo dose calculation system for photon beams on a water phantom.* Med. Phys., 2001. **28**: p. 1322–1337.
16. Neuenschwander, H., T.R. Mackie, and P.J. Reckwerdt, *MMC--a high-performance Monte Carlo code for electron beam treatment planning.* Phys Med Biol, 1995. **40**(4): p. 543-74.
17. Rogers, D.W., et al., *BEAM: a Monte Carlo code to simulate radiotherapy treatment units.* Med Phys, 1995. **22**(5): p. 503-24.
18. Reynaert, N., et al., *Monte Carlo treatment planning for photon and electron beams.* Radiation Physics and Chemistry, 2007. **76**(4): p. 44.
19. Chetty, I.J., et al., *Report of the AAPM Task Group No. 105: Issues associated with clinical implementation of Monte Carlo-based photon and electron external beam treatment planning.* Med Phys, 2007. **34**(12): p. 4818-53.
20. Rogers, D.W., *Fifty years of Monte Carlo simulations for medical physics.* Phys Med Biol, 2006. **51**(13): p. R287-301.
21. Otto, K., *Volumetric modulated arc therapy: IMRT in a single gantry arc.* Med Phys, 2008. **35**(1): p. 310-7.

22. Lobo, J. and I.A. Popescu, *Two new DOSXYZnrc sources for 4D Monte Carlo simulations of continuously variable beam configurations, with applications to RapidArc, VMAT, TomoTherapy and CyberKnife.* Phys Med Biol, 2010. **55**(16): p. 4431-43.
23. Shepard, D.M., et al., *Direct aperture optimization: a turnkey solution for step-and-shoot IMRT.* Medical Physics, 2002. **29**(6): p. 1007-18.
24. Bergman, A.M., et al., *Direct aperture optimization for IMRT using Monte Carlo generated beamlets.* Medical Physics, 2006. **33**(10): p. 3666-79.
25. Arrans, R., et al., *Computer optimization of class solutions designed on a beam segmentation basis.* Radiother Oncol, 2003. **69**(3): p. 315-21.
26. De Gersem, W., et al., *An anatomy-based beam segmentation tool for intensity-modulated radiation therapy and its application to head-and-neck cancer.* Int J Radiat Oncol Biol Phys, 2001. **51**(3): p. 849-59.
27. Rao, M., et al., *Comparison of anatomy-based, fluence-based and aperture-based treatment planning approaches for VMAT.* Physics In Medicine And Biology, 2010. **55**(21): p. 6475-90.
28. Craft, D., et al., *An approach for practical multiobjective IMRT treatment planning.* Int J Radiat Oncol Biol Phys, 2007. **69**(5): p. 1600-7.
29. Halabi, T., D. Craft, and T. Bortfeld, *Dose-volume objectives in multi-criteria optimization.* Phys Med Biol, 2006. **51**(15): p. 3809-18.
30. Romeijn, H.E., et al., *A novel linear programming approach to fluence map optimization for intensity modulated radiation therapy treatment planning.* Phys Med Biol, 2003. **48**(21): p. 3521-42.
31. Zhang, H.H., et al., *A two-stage sequential linear programming approach to IMRT dose optimization.* Phys Med Biol, 2010. **55**(3): p. 883-902.
32. Shepard, D.M., et al., *Optimizing the Delivery of Radiation Therapy to Cancer Patients.* SIAM, 1999. **41**(4): p. 24.
33. Salguero, F.J., et al., *Modulated electron radiotherapy treatment planning using a photon multileaf collimator for post-mastectomized chest walls.* Radiother Oncol, 2009. **93**(3): p. 625-32.
34. Palma, B.A., et al., *Combined modulated electron and photon beams planned by a Monte-Carlo-based optimization procedure for accelerated partial breast irradiation.* Phys Med Biol, 2012. **57**(5): p. 1191-202.
35. Cameron, C., *Sweeping-window arc therapy: an implementation of rotational IMRT with automatic beam-weight calculation.* Physics In Medicine And Biology, 2005. **50**(18): p. 4317-36.
36. Kawrakow, I., et al., *The EGSnrc Code System: Monte Carlo Simulation of Electron and Photon Transport*, in *NRCC Report PIRS-701*. 2011, National Research Council of Canada.
37. Rogers, D.W.O., B. Walters, and I. Kawrakow, *BEAMnrc Users Manual*, in *NRCC Report* 2011, National Research Council of Canada.
38. Walters, B., I. Kawrakow, and D. Rogers, *DOSXYZnrc User's Manual*, in *NRCC report PIRS 794*. 2005, National Research Council of Canada: Ottawa.
39. Ma, C., et al., *Monitor unit calculation for Monte Carlo treatment planning.* Physics in medicine and biology, 2004. **49**(9): p. 1671.
40. Czyzyk, J., et al., *PCx: An interior-point code for linear programming.* OPTIMIZATION METHODS & SOFTWARE, 1999. **11-2**(1-4): p. 397-430.
41. Deasy, J.O., A.I. Blanco, and V.H. Clark, *CERR: a computational environment for radiotherapy research.* Medical physics, 2003. **30**: p. 979.
42. El Naqa, I., et al., *A comparison of Monte Carlo dose calculation denoising techniques.* Physics In Medicine And Biology, 2005. **50**(5): p. 909-22.
43. Leal, A., et al., *Monte Carlo simulation of complex radiotherapy treatments.* COMPUTING IN SCIENCE & ENGINEERING, 2004. **6**(4): p. 60-68.

44. *NSABP B-39, RTOG 0413: A Randomized Phase III Study of conventional whole breast irradiation versus partial breast irradiation for women with stage 0, I, or II breast cancer.* Clin Adv Hematol Oncol, 2006. **4**(10): p. 719-21.
45. Miao, B., et al., *Adaptive anisotropic diffusion filtering of Monte Carlo dose distributions.* Physics In Medicine And Biology, 2003. **48**(17): p. 2767-81.
46. Thorwarth, D., et al., *Hypoxia dose painting by numbers: a planning study.* International Journal Of Radiation Oncology, Biology, Physics, 2007. **68**(1): p. 291-300.

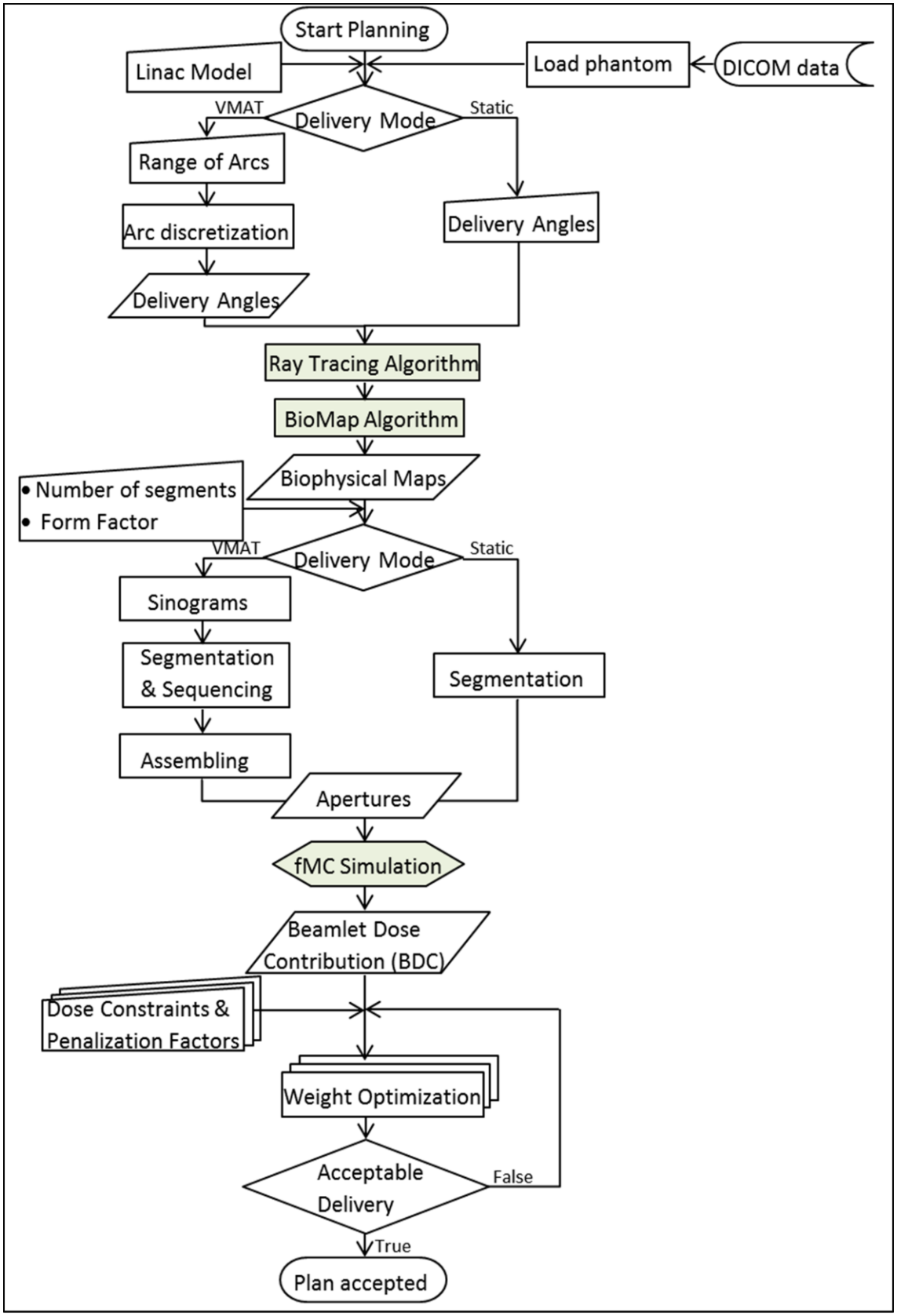

FIG. 1. CARMEN planning system workflow.

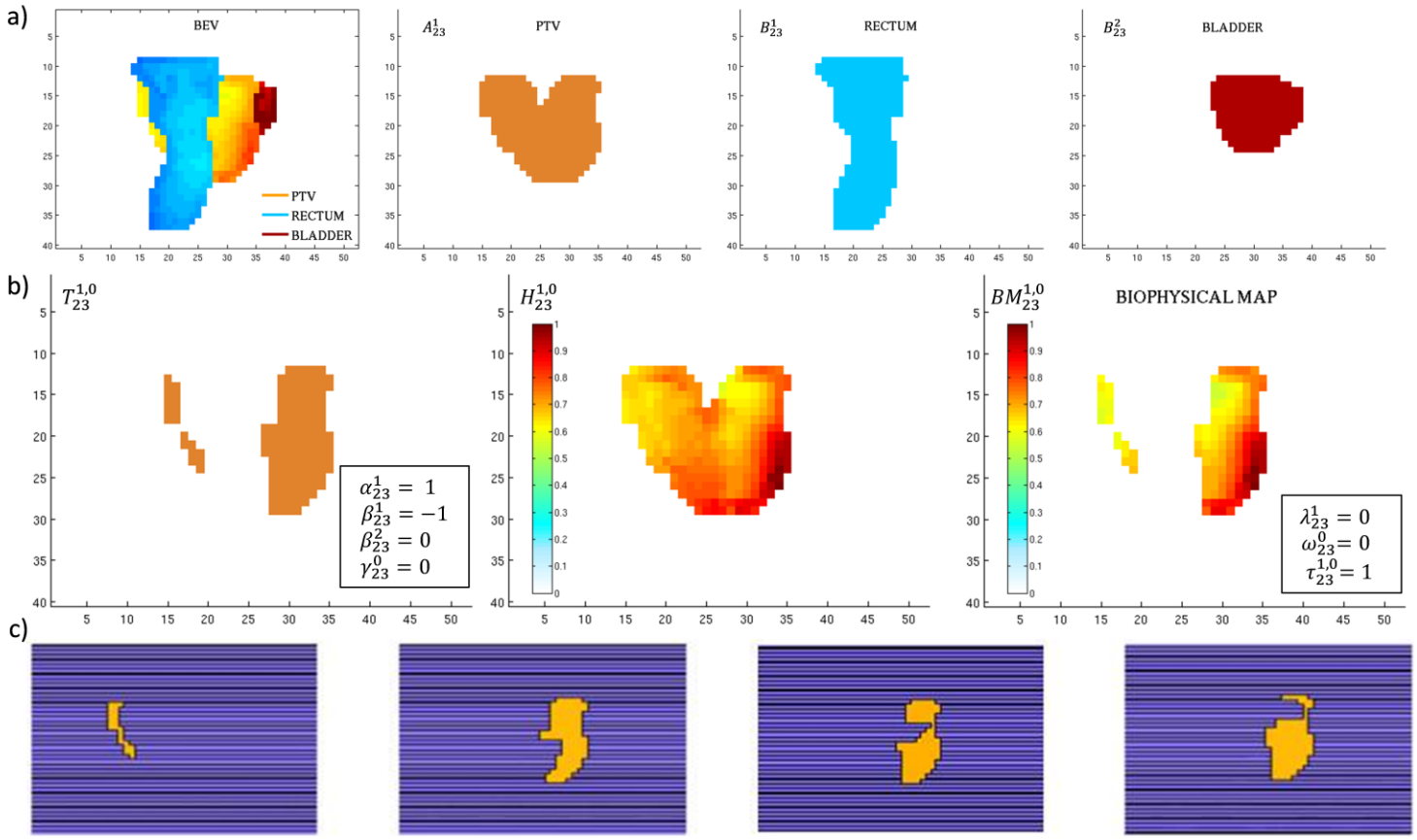

FIG. 2. For incidence 23 (220°), as an example, ray casting algorithm provides one Target (*l*=1), two OARs (m=1, 2), and no PET values (*r*=0). In a) the different structures with the corresponding matrices to be combined are shown. In b) are presented the matrices needed to generate the corresponding biophysical map and the latter in the right side. In c) are represented the apertures obtained with the sequencer. Form factor was strongly considered, the number of levels was set to 3 and the number of segments per level was set to 2.

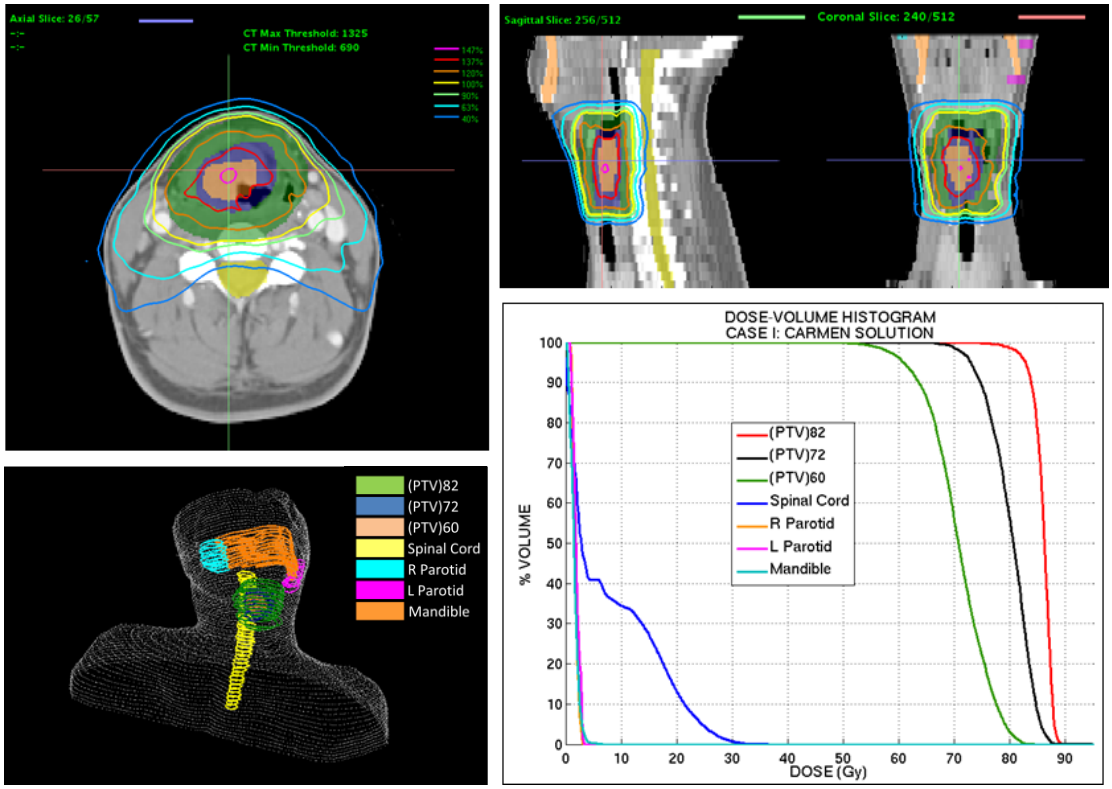

FIG. 3. Dose distributions showing the isolines of 40, 63, 90, 100, 120, 137 and 147% (24, 37.8, 54, 60, 72, 82.2, 88.2 Gy) at the isocenter slice and dose volume histogram obtained with CARMEN for case I.

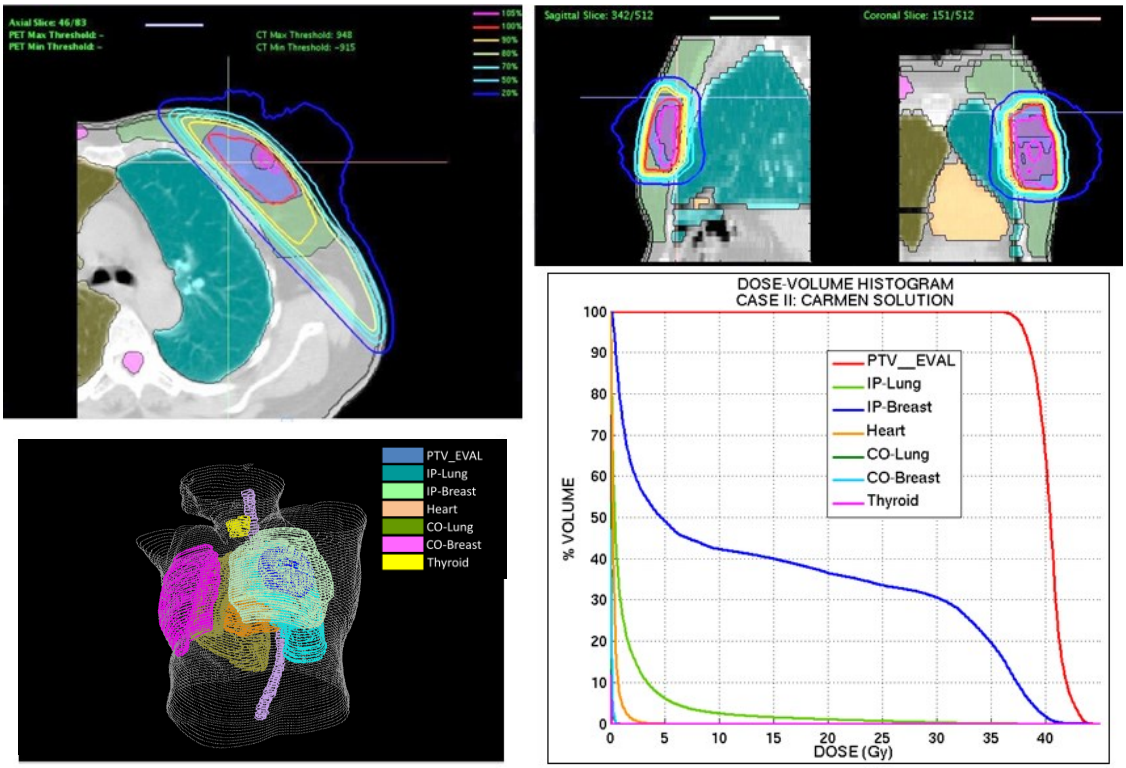

FIG. 4. Dose distributions showing the isolines of 20, 50, 70, 80, 90, 100 and 105% (7.7,19.25, 26.95, 30.8, 38.5, 40.425 Gy) at the isocenter slice and dose volume histogram obtained with CARMEN for case II.

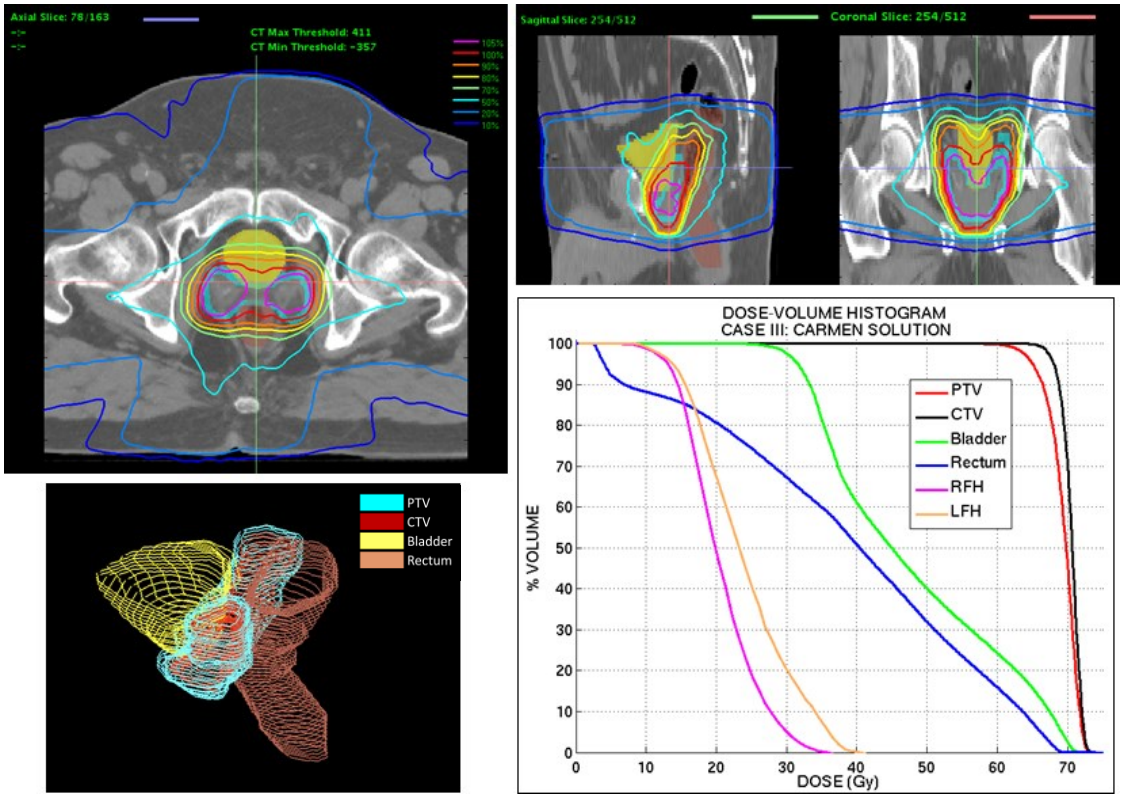

FIG. 5. Dose distributions showing the isolines of 10, 20, 50, 70, 80, 90, 100 and 105% (6.6, 13.2, 33, 46.2, 52.8, 59.4, 66, 69.3 Gy) at the isocenter slice and dose volume histogram obtained with CARMEN for case III.

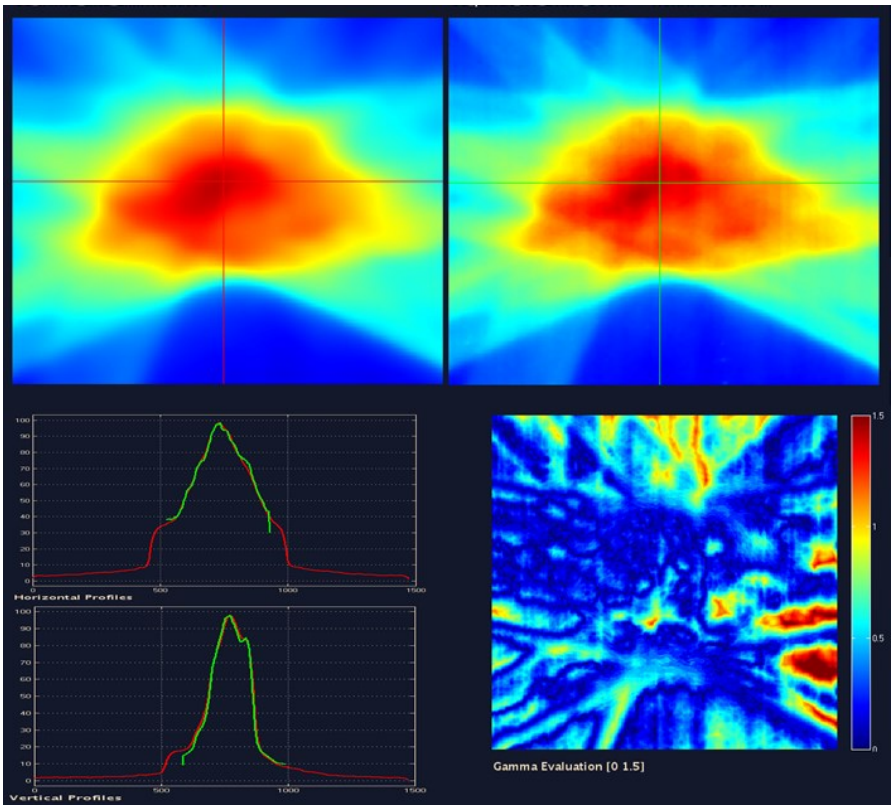

FIG. 6. QA report for case I. Dose distributions corresponding to MC solution (upper left) and to the film (upper right) at the isocenter slice; horizontal and vertical profiles (bottom left) and the corresponding gamma analysis (bottom right).

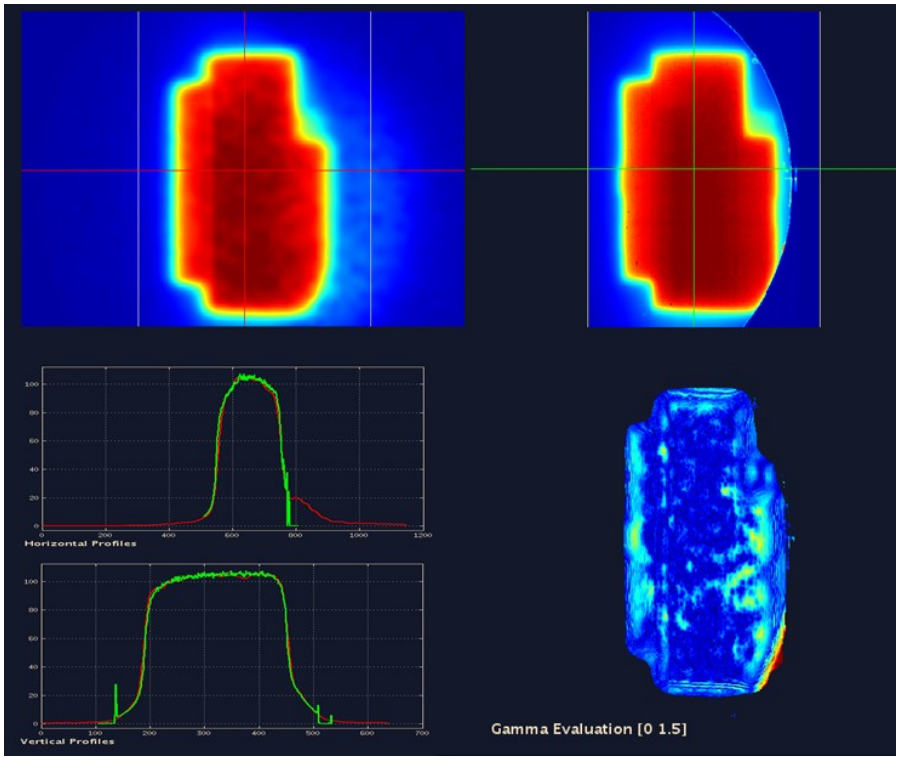

FIG. 7. QA report for case II. Dose distributions corresponding to MC solution (upper left) and to the film (upper right) at a representative slice; horizontal and vertical profiles (bottom left) and the corresponding gamma analysis (bottom right).

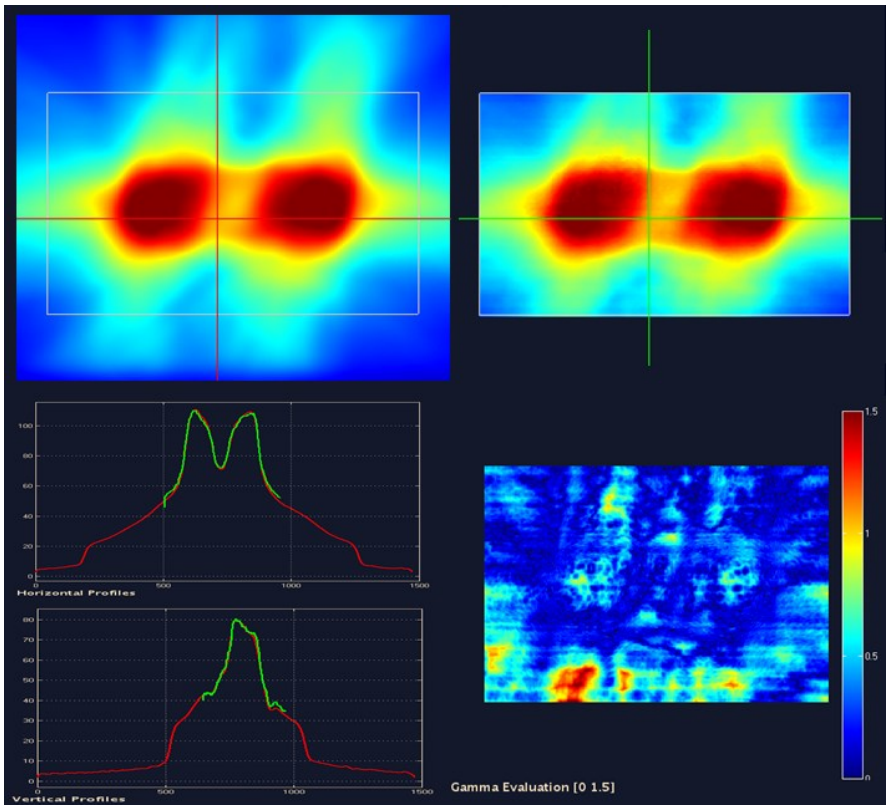

FIG. 8. QA report for case III. Dose distributions corresponding to MC solution (upper left) and to the film (upper right) at 3 cm off isocenter; horizontal and vertical profiles (bottom left) and the corresponding gamma analysis (bottom right).

TABLE I. Multiple dose prescription for case I: HR (Hypoxic Region – PTV82), PTV72, PTV60 and dose constraints for the organs at risk.

Prescribed dose and constraints, case I	
HR (PTV82); D_{95}	$\geq$ 136.7% D_p (82 Gy)
PTV72; D_{95}	$\geq$ 120% D_p (72 Gy)
PTV60; D_{95}	$\geq D_p$ (60 Gy)
Spinal cord; V_{38Gy} (63.3% D_p)	0%
Left Parotid gland; V_{38Gy} (63.3% D_p)	$\leq$ 5%
Right Parotid gland; V_{38Gy} (63.3% D_p)	$\leq$ 5%
Mandible; V_{30Gy} (50% D_p)	$\leq$ 1%

D_y is the dose delivered to y% of the structure volume, V_{xGy} is the volume receiving more than x Gy. D_p is the prescribed dose (60 Gy).

TABLE II. Dose prescription for case II and dose constraints with a 5% of tolerance according to the NSABP-B39/RTOG-0413 protocol.

Prescribed dose and constraints, case II	
PTV_EVAL;	
D_{90}	$\geq$ 90% D_p (34.7 Gy)
Dmax	$\leq$ 120% D_p (46.2 Gy)
Ipsilateral Breast	
$V_{19.3Gy}$ (50% D_p)	< 60%
$V_{38.5Gy}$ (100% D_p)	< 35%
Contralateral Breast; $V_{1.2Gy}$ (3% D_p)	0%
Ipsilateral Lung; $V_{11.6Gy}$ (30% D_p)	< 15%
Contralateral Lung; $V_{1.9Gy}$ (5% D_p)	< 15%
Heart; $V_{1.9Gy}$ (5% D_p)	< 40%
Thyroid; $V_{1.2Gy}$ (3% D_p)	0%

PTV_EVAL is the planning target volume used for evaluation, D_y is the dose delivered to y% of the structure volume, V_{xGy} is the volume receiving more than x Gy. D_p is the prescribed dose (38.5 Gy). Tolerance ±5%

TABLE III. Dose prescription and dose constraints for case III.

Prescribed dose and constraints, case III	
PTV; D_{95}	$\geq$ 95% D_p (62.7 Gy)
Bladder; $V_{46.2Gy}$ (70% D_p)	< 50%
Rectum; $V_{59.4Gy}$ (90% D_p)	< 20%
Rectum; $V_{39.6Gy}$ (60% D_p)	< 60%
Femoral Heads (RHF, LHF); V_{45Gy} (68.2%D_p)	0%

D_y is the dose delivered to y% of the structure volume, V_{xGy} is the volume receiving more than x Gy. D_p prescribed dose (66 Gy).

TABLE IV. Dosimetric values planned by CARMEN for case I: HR (Hypoxic Region – PTV82), PTV72, PTV60 and dose constraints for the organs at risk; for case II and dose constraints with a 5% of tolerance according to the NSABP-B39/RTOG-0413 protocol and for case III and dose constraints.

CASE I		CASE II		CASE III	
HR (PTV82)	D_{95} = 83.2 Gy	PTV_EVAL	D_{95} = 38.1 Gy	PTV	D_{95} = 65.0 Gy
8.0 cm^3	D_2 = 88.5 Gy	166.0 cm^3	D_{max} = 44.3 Gy	98.0 cm^3	D_2 = 70.2 Gy
	D_{98} = 86.4 Gy		D_2 = 43.2 Gy		D_{98} = 63.4 Gy
	D_{mean} = 86.0 Gy		D_{98} = 37.3 Gy		D_{mean} = 69.4 Gy
	CI = 0.996		D_{mean} = 40.4 Gy		CI = 0.988
			CI = 0.994		
PTV72	D_{95} = 73.4 Gy	Ipsilat. Breast	$V_{19.3Gy}$ = 37.2%	Bladder	$V_{46.2Gy}$ = 46.4 %
21.3 cm^3	D_2 = 86.4 Gy		$V_{38.5Gy}$ = 5.5%		D_2 = 70.2 Gy
	D_{98} = 71.8 Gy		D_2 = 39.8 Gy		D_{mean} = 47.5 Gy
	D_{mean} = 80.2 Gy		D_{mean} = 14.6 Gy		
	CI = 0.998				
PTV60	D_{95} = 61.0 Gy	Contralateral Breast	$V_{1.2Gy}$ = 0%	Rectum	$V_{59.4Gy}$ = 17.8%
108.8 cm^3	D_2 = 80.6 Gy		D_2 = 0.5 Gy		$V_{38.6Gy}$ = 52.9%
	D_{98} = 57.9 Gy		D_{mean} = 0.1 Gy		D_2 = 67.9 Gy
	D_{mean} = 70.6 Gy				D_{mean} = 39.1 Gy
	CI = 0.984				
Spinal cord	V_{38Gy} = 0%	Ipsilateral Lung	$V_{11.6Gy}$ = 2.2%	Right Femoral Head	V_{45Gy} = 0%
	D_2 = 28.8 Gy		D_2 = 12.6 Gy		D_2 = 31.5 Gy
	D_{mean} = 8.4Gy		D_{mean} = 1.6 Gy		D_{mean} = 20.1 Gy
		Contralateral Lung	$V_{1.9Gy}$ = 0%	Left Femoral Head	V_{45Gy} = 0%
			D_2 = 0.4 Gy		D_2 = 36.5 Gy
			D_{mean} = 0.1 Gy		D_{mean} = 23.4 Gy
Left Parotid gland	V_{38Gy} = 0%	Heart	$V_{1.9Gy}$ = 1.5%		
	D_2 = 3.3 Gy		D_2 = 1.7 Gy		
	D_{mean} = 2.1 Gy		D_{mean} = 0.5 Gy		
Right Parotid gland	V_{38Gy} = 0%	Thyroid	$V_{1.2Gy}$ = 0%		
	D_2 = 3.1 Gy		D_2 = 0.1 Gy		
	D_{mean} = 2.0 Gy		D_{mean} = 0.1 Gy		
Mandible	V_{30Gy} = 0%				
	D_2 = 3.7 Gy				
	D_{mean} = 1.8 Gy				

D_y is the percentage of prescribed dose delivered to y% of the structure volume, V_{xGy} is the volume percentage receiving more than x Gy. D_p is the prescribed dose (60 Gy). CI conformity index (V_{95}/V_{target}).

TABLE V . Planning parameters of CARMEN for the three evaluated cases.

	Planning System	Energy	Gantry Angles	Segments (weight ≠ 0)	MU
Case I	CARMEN (ph)	6 MV	0º, 40º, 80º, 120º, 160º, 200º, 240º, 280º, 320º	140 (69)	579.0
Case II	CARMEN (elec + ph)	9 MeV/ 6 MV	25º, 40º/139º, 317º	5	520.0
Case III	CARMEN (ph)	6 MV	1 arc of 356º (3min. 5 sec.)	180 (117)	375.0

TABLE VI . Absolute dose verification and global gamma analysis for the three presented cases.

	Experimental dose (cGy)	MC dose (cGy)	Relative error (%) $\frac{D_{MC}-D_{exp}}{D_{exp}}$	Global gamma (%) (3% / 3mm)		
Case I	221.20	226.90	+2.60	96.04	99.53	
Case II	366.61	366.18	- 0.12	97.45	99.18	97.38
Case III	216.10	216.50	+0.16	96.64	96.15	98.56

D_{MC} is the estimated MC dose, D_{exp} is the measured dose.

TABLE VII . Times spent by the CARMEN system for each planning stage of the cases.

	Apertures generation	Apertures simulation (PSDs)	Dose calculation	Optimization	Total time
Case I	14 min	55 min	18 min	30 min	117 min
Case II	7 min	15 min	30 min	3 min	55 min
Case III	28 min	60 min	56 min	25 min	169 min